ANALYSIS AND DESIGN OF A PIEZOELECTRIC MICRO-ACTUATOR

by

PO-SHIUN CHEN

Presented to the Faculty of the Graduate School of

The University of Texas at Arlington in Partial Fulfillment

of the Requirements

for the Degree of

MASTER OF SCIENCE IN MECHANICAL ENGINEERING

THE UNIVERSITY OF TEXAS AT ARLINGTON

AUGUST 2006

ACKNOWLEDGEMENTS

During the long period to complete this thesis, I would sincerely like to acknowledge many people who contributed to this thesis in particular. I want to gratefully thank my thesis advisor, Dr. Panayiotis S. Shiakolas, who provided his time, constructive criticisms and invaluable ideas during my study. I would like to thank my thesis committee members, Dr. Kent L. Lawrence and Shashank Priya, for their time and suggestions.

Also, I want to thank my colleagues, Nitin Uppal, Sunil Belligundu, Venkat Raghavan, Tony Chang, Gianfranco Rios, and Rachmat sofian who work or study in the BioMEMS and MARS laboratories and whose ideas and friendships support me to complete this thesis.

In addition, I want to thank my parents, sisters, and friends no matter in Taiwan or in U.S.A. Your love and support propel and strengthen me forever.

June 26, 2006

ABSTRACT

ANALYSIS AND DESIGN OF A PIEZOELECTRIC

MICRO-ACTUATOR

Publication No. _____

Po-Shiun Chen, MS

The University of Texas at Arlington, 2006

Supervising Professor: Dr. Panayiotis S. Shiakolas

Micro-grippers are usually fabricated of silicon using traditional semiconductor manufacturing processes and actuated based on thermal energy input causing their temperature to substantially increase and render unsuitable for certain applications such as biological tissue handling. In this research work, the design of a micro-gripper using piezoelectric ceramics (PZT) is presented as an alternative to silicon based micro gripper. The design procedure utilized ANSYS, a Finite Element Method based software tool to verify simple PZT models and subsequently evaluate the stroke for a family of configurations. The configurations were further explored and optimized

considering that the fabrication would be performed using the femtosecond laser micro machining system available in our laboratory for further testing and characterization.

TABLE OF CONTENTS

LIST OF ILLUSTRATIONS

LIST OF TABLES

CHAPTER 1

INTRODUCTION

Over the past decades, micro-electro-mechanical systems (MEMS) have been developed for the medical, automotive, robotics and other fields. The applications include chemical sensors, acceleration transducers, pressure transducers, micro grippers, micro X-Y stages, micro-valves and so on. The primary design parameters for micro actuators are displacement, force, frequency, weight, size, power consumption, speed, and power density and the ones to concentrate on during the design process depend on the application. A micro gripper is an important device to be used as a micro knife in bio research or assembly of components for micro machines. In this research work, different configurations of micro grippers/actuators are discussed based on piezoceramic materials with the notion that the completed design is to be fabricated using a Femtosecond Laser Mircomachining System housed in the BioMEMS laboratory of the department of Mechanical and Aerospace Engineering of The University of Texas at Arlington. [1]

The procedures and concepts to be discussed in this research work could be easily followed and repeated for the design of new micro gripper should new piezoelectric materials are discovered in order to simulate and evaluate their

performance. The primary design parameters, concepts, and applied voltages, the actuators with new material properties could possibly generate larger deflections.

Typically, the technology used in MEMS gripper can be described as four main fields which are thermal, Shape Memory Alloys (SMA), electrostatic, piezoelectric actuators. In general, most actuators execute well in some fields but poor in others. For example, electro-thermal actuators are known for their excellent large defection and force, but traditionally the temperature of the structure is high. Also, typical Shape Memory Alloys (SMA) including combinations of metal elements such as TiNi ("Nitinol") have advantages like high power density, but they are mainly affected by and greatly depend on the surrounding temperature conditions. So, both of electro-thermal actuator and SMA require cooling system to reverse their action. [2] On the other hand, the advantages of the electrostatic actuator are small actuation energy and high frequency response, and the disadvantages are high driving voltage, large working area and low output force. [3] The following section will introduce and discuss the advantages and disadvantages of the micro gripper when different various methods are used to transform energy into motion.

1.1 Thermal

There are two basic actuators for thermal MEMS, and because of the structures, one of them is described as cold and hot arm (Fig. 1 (a)) [4], and another one is buckle beam (Fig. 1(b)) [3].Usually, buckle beam actuator can generate large force (450 uN/mm^2) and displacement in a compact size by heating the structure. [4] In addition, when operating the actuator, the deformation in the thin part is larger than the

deformation in the wide part. Though, it can generate high output force by low voltages, but the temperature generated by thermal actuator would be extremely high which can reach more than $800^{\circ}C$ (Fig. 2). [4] The advantages of this actuator are that it can be fabricated easily and generate large force and deflection by low voltage, and needs smaller chip area. But the disadvantage is the generated temperature is so high that it could need passive or active cooling system to reduce the temperature for certain applications of high bandwidth. [2]

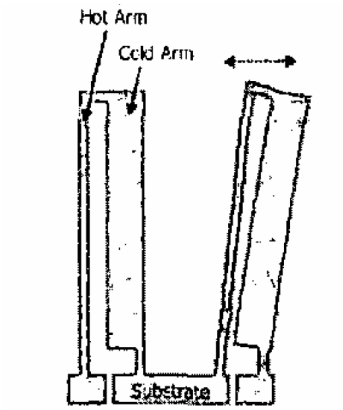

(a)

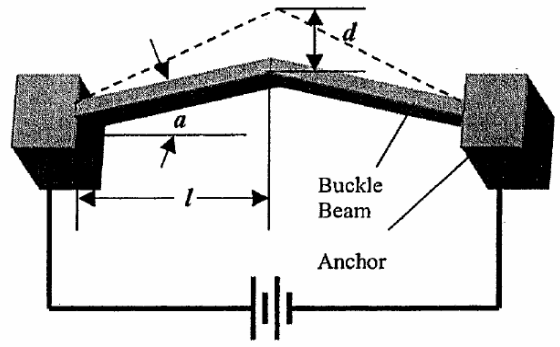

(b)

Fig. 1 Two thermal actuators (a) cold and hot arm [4] (b) buckle beam [3]

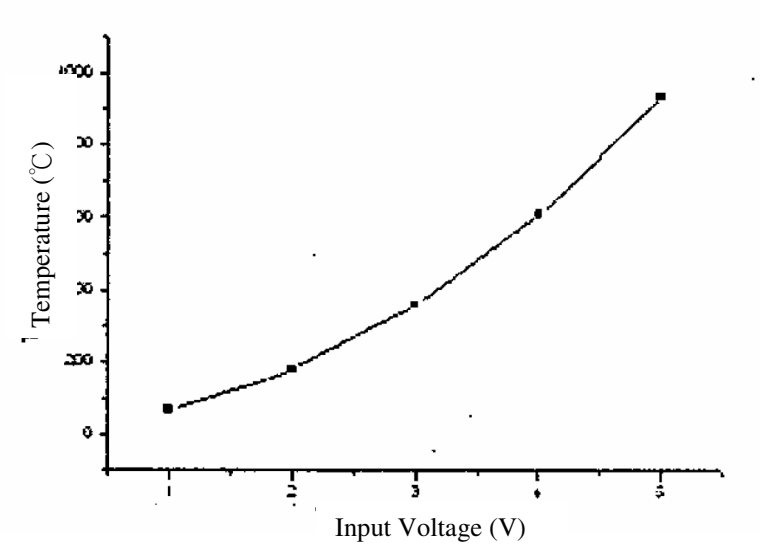

Fig. 2 The maximum temperature of structure vs. input voltage. [4]

1.2 Shape Memory Alloys (SMA)

SMA thin film is fabricated by sputtering deposition. At high temperature substrate condition, the TiNi film will be crystallized in regular crystal, and at low substrate temperature, the amorphous structure will appear. Therefore, when SMA is set to be bending shape at high temperature, and to be linear shape at the amorphous temperature, it will be deformed by passing current (Fig. 3). [5] SMA actuator generally generates a very high force with low driving voltage but has a low efficiency in converting electrical energy to motion. As thermal actuator, SMA actuator is affected by surrounding temperature condition, and also requires cooling system to reverse the deformation. [2]

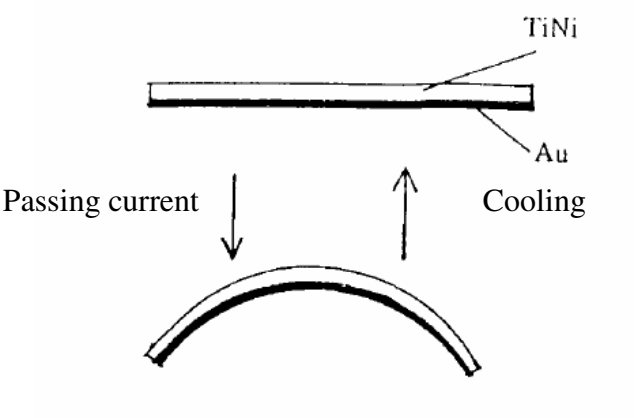

Fig. 3 Two way bending behavior of the bimetal thin film composed of TiNi and gold [5]

1.3 Electrostatic

The electrostatic actuator has become one of the main actuation technologies employed. The motion of the electrostatic actuator is due to electrostatic repulsion by image charges mirrored in the ground plane beneath the suspended structure. By electrically isolating alternating drive-comb fingers (Fig. 4) and applying voltages of equal magnitude and opposite sign, levitation can be reduced by an order of magnitude, while reducing the lateral drive force by less than a factor or two as showed in Fig. 5 (a) and (b). [6] This kind of actuator has small actuation energy and high frequency response, but it also has drawbacks such as high driving voltage, large working area (high number of teeth), and low output force. [3] In addition, with the pull-in effect, when the displacement is higher than 1/3 of the gap, the displacement is nonlinear. To reverse this situation, it often operates with a feedback loop system. [7]

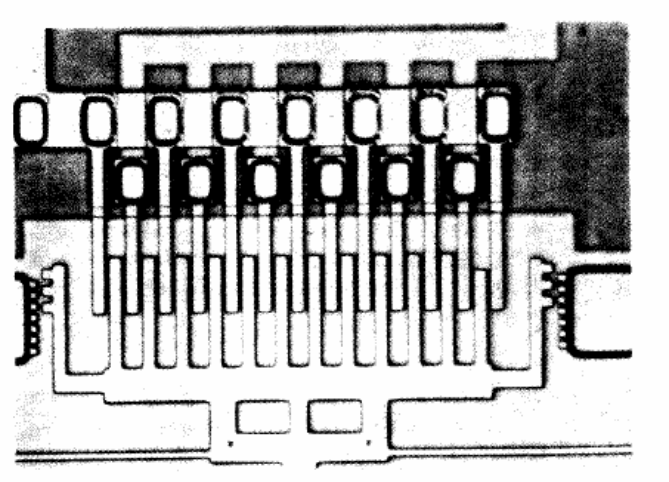

Fig. 4 Comb drive device – moving finger translates vertically [6]

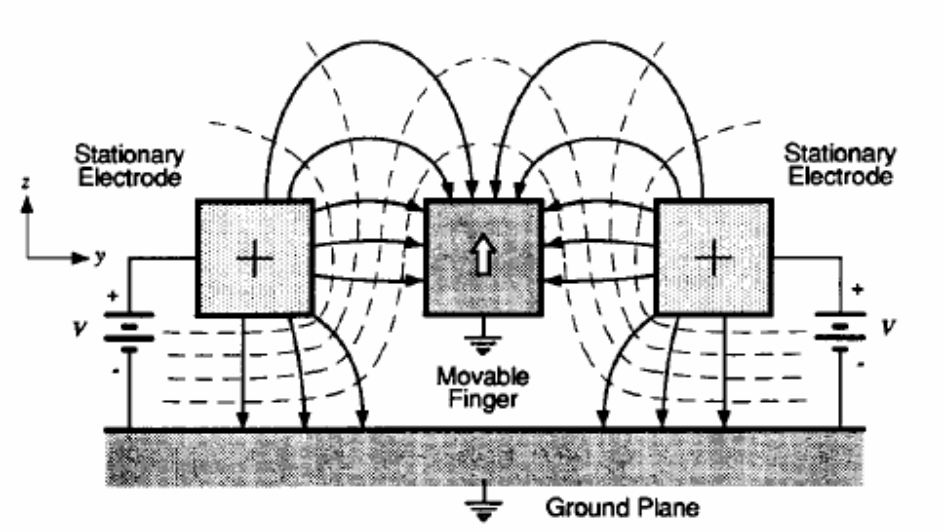

(a)

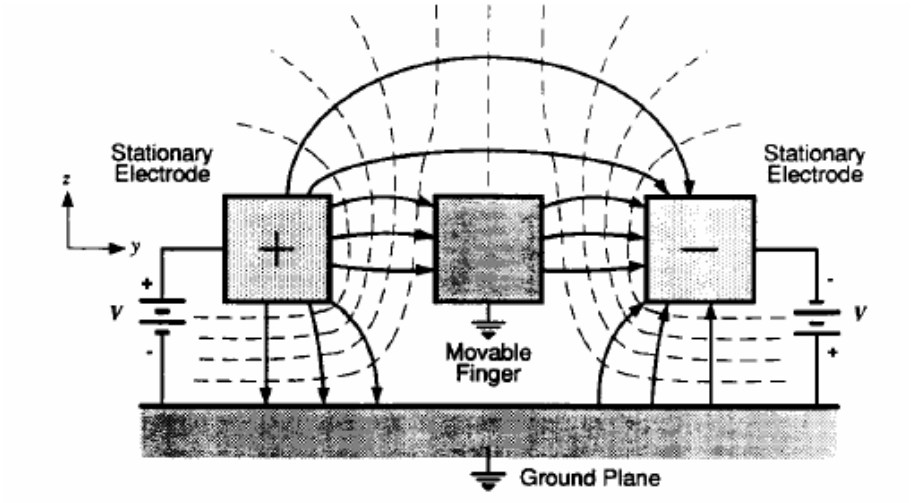

(b)

Fig. 5 (a) Cross section of the gripper when same voltage is applied on electrodes (b) Cross section of the gripper when opposing voltage is applied on electrodes. [6]

1.4 Piezoelectric

Main piezoelectric materials used in MEMS include Lead Zirconate Titanate (PZT), Zinc Oxide (ZnO), Aluminum Nitride (AIN), Quartz (SiO2), Poly-Vinylidene Fluoride (PVDF) and so on. When the piezoelectric material is excited by voltage, the asymmetric lattice structure creates strains in length, width, and thickness directions (Fig. 6). [8] Piezoelectric actuation architectures generally can be described as three different schemes: externally leveraged (Fig. 7), internally leveraged (Fig. 8), and frequency leveraged (Fig. 9). [9] Externally leveraged actuators rely on an external mechanical component for the actuating ability. Internally leveraged actuators generate amplified strokes through internal structure without using the external mechanical component. Frequency leveraged actuators rely on an alternating control signal to generate motion. [9][10]

Piezoelectric actuators have excellent operating bandwidth and large forces, high power density, and well reversion, but the displacements generated are so small that the piezoelectric research focuses on developing an architecture that can generate high displacement. Therefore, novel concepts are developed and explored during the design process to overcome the stroke limitation of the material.

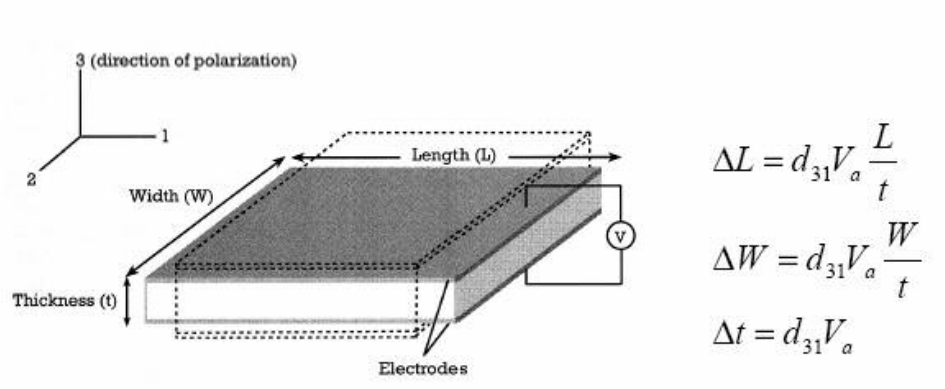

Fig. 6 The deformation and simply equations of the piezoelectric material [8]

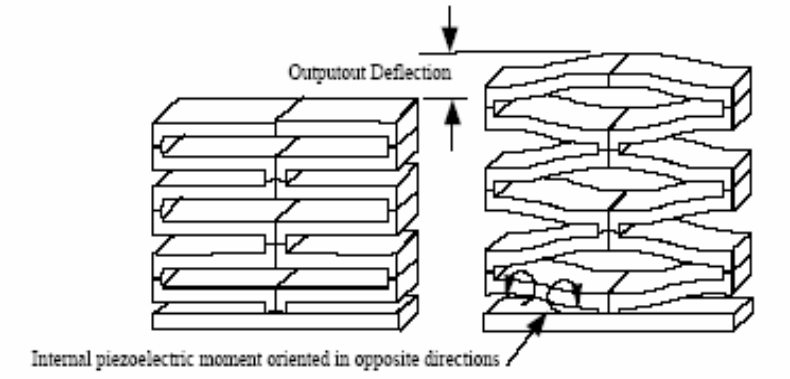

Fig. 7 Internally leveraged actuators [9]

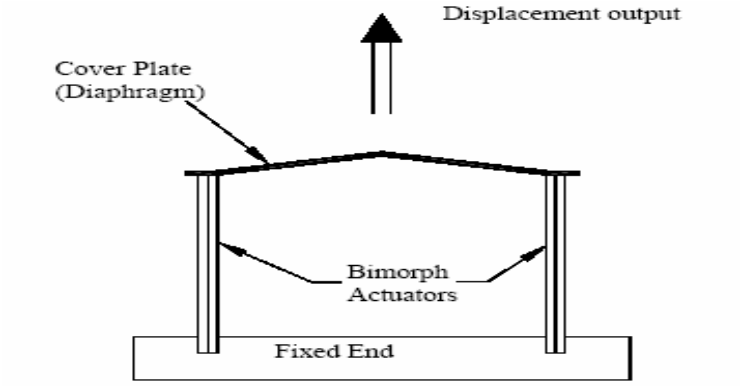

Fig. 8 Externally leveraged actuators [9]

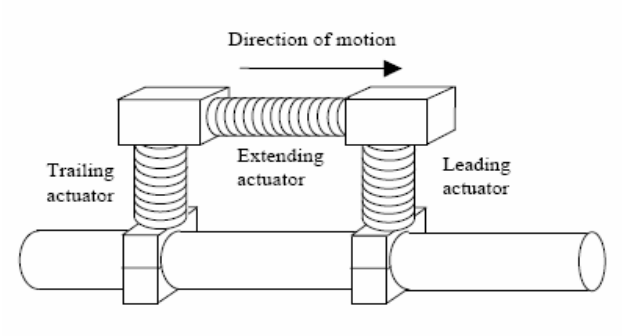

Fig. 9 Frequency leveraged actuators [9]

1.5 Comparison Table

A qualitative comparison for the four micro-actuator technologies is presented in Table 1. [2][7]

Table 1 Comparison for Four Micro-Actuator Technologies [2] [7]

Actuator Method	Efficiency	Temperature Sensitivity	Speed	Power Density
Thermal	Very high	Yes	Medium	Medium
Shape Memory Alloy	Low	Yes	Medium	Very high
Electrostatic	Very high	No	Fast	High
Piezoelectric	Very high	No	Fast	High

In this research work, Chapter 2 will introduce material from piezoelectric theory and the simulation tools and procedures followed. Chapter 3 will discuss the modeling process, the performance of the various micro gripper/actuator design concepts and the sensitivity of the displacement due to changes on geometric parameters and optimization results. The conclusions and recommendations for future expansion will be discussed in Chapter 4. A sample file used in the finite element analysis software ANSYS is presented in Appendix B.

CHAPTER 2

PIEZOELECTRIC MATERIAL PROPERTIES AND MODELING TOOLS

2.1 Piezoelectric Material Properties

Recently, several piezoelectric materials including, Lead Titanate Zirconate ceramics (PZT-4, PZT-5A, PZT-5H, PZT-7A etc.), Barium Titanate, and Polyvinylidene Flouride have been investigated and characterized. [8] In this study, PZT was selected as the piezoelectric material because of its high piezoelectric and dielectric constants. Initially, a brief description of piezoelectric theory is presented to summarize the important relationships. The constitutive equations (1) and (2) describe the interrelationship among the external variable and piezoelectric coefficients. [11]

$$S = d \cdot E \qquad \text{Strain} \qquad (1)$$

$$D = Q/A = d \cdot T \qquad \text{Dielectric charge} \qquad (2)$$

Equations (3) and (4) show the coupled relationship of the strain and charge. The symbols are defined as piezoelectric strain (S), applied stress (T), dielectric displacement (D), applied electric field (E), and piezoelectric strain constant, d. The superscripts describe the conditions under which the material property data was measured. For example, the superscript E on the compliance matrix s^E means that the compliance data was measured under constant electric field condition.

$$S = s^E \cdot T + d^t \cdot E \qquad (3)$$

$$D = d \cdot T + \varepsilon^T \cdot E \tag{4}$$

From the strain-charge, stress-charge, strain-voltage, and stress voltage form, the relationships for piezoelectric material can be easily derived as shown in Table 2. [13]

Table 2 Four Forms for Piezoelectric Constitutive Equations [12]

Strain-Charge Form	Strain-Voltage Form	Stress-Charge Form	Stress-Voltage Form
$S = s^E \cdot T + d^t \cdot E$ $D = d \cdot T + \varepsilon^T \cdot E$	$S = s^D \cdot T + g^t \cdot D$ $E = -g \cdot T + \varepsilon^{T^{-1}} \cdot D$	$T = c^E \cdot S - e^t \cdot E$ $D = e \cdot S + \varepsilon^S \cdot E$	$T = c^D \cdot S - q^t \cdot D$ $E = -q \cdot S + \varepsilon^S \cdot E$

Matrix transformations for converting piezoelectric constitutive data from one form into another are shown in Table 3.

Table 3 Matrix Transformations for Piezoelectric Constitutive Data [12]

Strain-Charge To Stress-Charge	Strain-Voltage To Stress-Voltage
$c^E = s^{E^{-1}}$ $e = d \cdot s^{E^{-1}}$ $\varepsilon^S = \varepsilon^T - d \cdot s^{E^{-1}} \cdot d^t$	$c^D = s^{D^{-1}}$ $q = g \cdot s^{D^{-1}}$ $\varepsilon^{S^{-1}} = \varepsilon^{T^{-1}} + g \cdot s^{D^{-1}} \cdot g^t$
Strain-Charge To Strain-Voltage	Stress-Charge To Stress-Voltage
$s^D = s^E - d^t \cdot \varepsilon^{T^{-1}} \cdot d$ $g = \varepsilon^{T^{-1}} \cdot d$	$c^D = c^E + e^t \cdot \varepsilon^{S^{-1}} \cdot e$ $q = \varepsilon^{S^{-1}} \cdot e$

The symbol definitions for the matrix transformations and the coupled equations presented in Table 2 and 3 are shown in Table 4.

Table 4 Piezo Symbol Definitions [12]

Symbol	Type	Matrix size	units	Description
T	Vector	6 x 1	$\frac{N}{m^2}$	stress components (e.g. σ_1)
S	Vector	6 x 1	$\frac{m}{m}$	strain components (e.g. ε_3)
E	Vector	3 x 1	$\frac{N}{C}$	electric field components
D	Vector	3 x 1	$\frac{C}{m^2}$	electric charge density displacement components
s	Matrix	6 x 6	$\frac{m^2}{N}$	Piezoelectric compliance coefficients
c	Matrix	6 x 6	$\frac{N}{m^2}$	stiffness coefficients
ε	Matrix	3 x 3	$\frac{F}{m}$	electric permittivity
d	Matrix	3 x 6	$\frac{C}{N}$	piezoelectric coupling coefficients for Strain-Charge form
e	Matrix	3 x 6	$\frac{C}{m^2}$	piezoelectric coupling coefficients for Stress-Charge form
g	Matrix	3 x 6	$\frac{m^2}{C}$	piezoelectric coupling coefficients for Strain-Voltage form
q	Matrix	3 x 6	$\frac{N}{C}$	piezoelectric coupling coefficients for Stress-Voltage form

The constitutive matrices for piezoelectric materials shown here are listed in the ANSI (IEEE) standards, by keeping polarization direction of the piezoelectric material along the Z-Axis in equations (5-8). The piezoelectric elastic compliance coefficient s^E (M^2/N), the piezoelectric strain coefficient d (C/N), and the piezoelectric permittivity ε are the critical parameters, and high values are desired for actuator

applications. The piezoelectric permittivity ε is a measure of the charge stored on an electrode material at a given voltage. The permittivity of vacuum is $\varepsilon_0 = 8.85 \cdot 10^{-12}\ F/M$. The relative permittivity is the ratio of ε_T and ε_0. [14] For cubic material the tensor matrices can be represented as following.

$$\varepsilon^T = \begin{bmatrix} \varepsilon_{11} & 0 & 0 \\ 0 & \varepsilon_{11} & 0 \\ 0 & 0 & \varepsilon_{33} \end{bmatrix}$$

Piezoelectric permittivity (dielectric constants) matrix is symmetric (5)

$$\frac{\varepsilon^T}{\varepsilon_0} = \begin{bmatrix} K_{11} & 0 & 0 \\ 0 & K_{11} & 0 \\ 0 & 0 & K_{33} \end{bmatrix}$$

Relative permittivity matrix is symmetric (6)

$$s^E = \begin{bmatrix} s_{11} & s_{12} & s_{13} & 0 & 0 & 0 \\ s_{12} & s_{11} & s_{13} & 0 & 0 & 0 \\ s_{13} & s_{13} & s_{33} & 0 & 0 & 0 \\ 0 & 0 & 0 & s_{44} & 0 & 0 \\ 0 & 0 & 0 & 0 & s_{44} & 0 \\ 0 & 0 & 0 & 0 & 0 & 2(s_{11}-s_{12}) \end{bmatrix}$$

Piezoelectric elastic compliance matrix is symmetric (7)

$$d = \begin{bmatrix} 0 & 0 & 0 & 0 & d_{15} & 0 \\ 0 & 0 & 0 & d_{15} & 0 & 0 \\ d_{31} & d_{31} & d_{33} & 0 & 0 & 0 \end{bmatrix} \quad \text{Piezoelectric strain coefficient} \qquad (8)$$

When three equations (5),(7), and(8) put into the constitutive equations (3)-(4), the specific equations (9)-(17) and relationships along the polarization-axis can be obtained. [14]

$$S_1 = s_{11}T_1 + s_{12}T_2 + s_{13}T_3 + d_{31}E_3 \qquad (9)$$

$$S_2 = s_{11}T_2 + s_{12}T_1 + s_{13}T_3 + d_{31}E_3 \qquad (10)$$

$$S_3 = s_{13}(T_1 + T_2) + s_{33}T_3 + d_{33}E_3 \qquad (11)$$

$$S_4 = s_{44}T_4 + d_{15}E_2 \qquad (12)$$

$$S_5 = s_{44}T_5 + d_{15}E_1 \qquad (13)$$

$$S_6 = s_{66}T_6 \qquad \left(s_{66} = 2(s_{11} - s_{12})\right) \qquad (14)$$

$$D_1 = \varepsilon_{11}E_1 + d_{15}T_5 \qquad (15)$$

$$D_2 = \varepsilon_{11}E_2 + d_{15}T_4 \qquad (16)$$

$$D_3 = \varepsilon_{33}E_3 + d_{31}(T_1 + T_2) + d_{33}T_3 \qquad (17)$$

2.2. Piezoelectric Material Simulation Methods and Tools

ANSYS was used to predict and optimize the performance of the actuator. Initially, the differences between IEEE and ANSYS standards in the parameters such as

piezoelectric elastic compliance s^E and piezoelectric strain coefficient d were addressed. [15]

The first step in using ANSYS for PZT analysis is to define three matrices: permittivity matrix (dielectric constants), piezoelectric strain (or stress) matrices, and elastic coefficient (or stiffness) matrices. The piezoelectric matrix can be in [e] form (piezoelectric stress matrix) or in [d] form (piezoelectric strain matrix). The [e] matrix is typically associated with the input of the anisotropic elasticity in the form of the stiffness matrix [c], while the [d] matrix is associated with the compliance matrix [s], where the stiffness matrix [c] is the inverse of the compliance matrix [s].

For most published piezoelectric materials, the order used for the piezoelectric matrix is [x, y, z, yz, xz, xy] based on IEEE standards, while the ANSYS input order is [x, y, z, xy, yz, xz]. This means that to transform the matrix to the ANSYS input order row data switching for the shear terms is needed. Equations 18 and 19 are the transformed matrices between IEEE and ANSYS.

IEEE constants [e_{61}, e_{62}, e_{63}] must be defined as ANSYS xy row, and IEEE constants [e_{41}, e_{42}, e_{43}] must be defined as ANSYS yz row, and IEEE constants [e_{51}, e_{52}, e_{53}] must be defined as ANSYS xz row.

$$[e]=\begin{array}{c} \\ x \\ y \\ z \\ xy \\ yz \\ xz \end{array}\begin{array}{c} \begin{array}{ccc} x & y & z \end{array} \\ \begin{bmatrix} e_{11} & e_{12} & e_{13} \\ e_{21} & e_{22} & e_{23} \\ e_{31} & e_{32} & e_{33} \\ e_{41} & e_{42} & e_{43} \\ e_{51} & e_{52} & e_{53} \\ e_{61} & e_{62} & e_{63} \end{bmatrix} \\ (3-D) \end{array} \quad [e]=\begin{array}{c} \begin{array}{cc} x & y \end{array} \\ \begin{bmatrix} e_{11} & e_{12} \\ e_{21} & e_{22} \\ e_{31} & e_{32} \\ e_{41} & e_{42} \end{bmatrix} \\ (2-D) \end{array}$$

$$\text{ANSYS } [e]=\begin{array}{c} \\ x \\ y \\ z \\ xy \\ yz \\ xz \end{array}\begin{array}{c} \begin{array}{ccc} x & y & z \end{array} \\ \begin{bmatrix} e_{11} & e_{12} & e_{13} \\ e_{21} & e_{22} & e_{23} \\ e_{31} & e_{32} & e_{33} \\ e_{61} & e_{62} & e_{63} \\ e_{41} & e_{42} & e_{43} \\ e_{51} & e_{52} & e_{53} \end{bmatrix} \end{array} \quad (18)[15]$$

IEEE terms [c_{61}, c_{62}, c_{63}, c_{66}] must be defined as ANSYS xy row, IEEE terms [c_{41}, c_{42}, c_{43}, c_{46}, c_{44}] must be defined as ANSYS yz row, and IEEE terms [c_{51}, c_{52}, c_{53}, c_{56}, c_{54}, c_{55}] must be defined as ANSYS xz row.

$$[c] = \begin{array}{c} \\ x \\ y \\ z \\ xy \\ yz \\ xz \end{array} \begin{array}{c} \begin{array}{cccccc} x & y & z & xy & yz & xz \end{array} \\ \begin{bmatrix} c_{11} & & & & & \\ c_{21} & c_{22} & & & & \\ c_{31} & c_{32} & c_{33} & & & \\ c_{41} & c_{42} & c_{43} & c_{44} & & \\ c_{51} & c_{52} & c_{53} & c_{54} & c_{55} & \\ c_{61} & c_{62} & c_{63} & c_{64} & c_{65} & c_{66} \end{bmatrix} \\ (3-D) \end{array} \qquad \begin{array}{c} \\ x \\ y \\ z \\ xy \end{array} \begin{array}{c} \begin{array}{cccc} x & y & z & xy \end{array} \\ \begin{bmatrix} c_{11} & & & \\ c_{21} & c_{22} & & \\ c_{31} & c_{32} & c_{33} & \\ c_{41} & c_{42} & c_{43} & c_{44} \end{bmatrix} \\ (2-D) \end{array}$$

$$ANSYS[c]^E = \begin{array}{c} \\ x \\ y \\ z \\ xy \\ yz \\ xz \end{array} \begin{array}{c} \begin{array}{cccccc} x & y & z & xy & yz & xz \end{array} \\ \begin{bmatrix} c_{11} & & & & & \\ c_{21} & c_{22} & & & & \\ c_{31} & c_{32} & c_{33} & & & \\ c_{61} & c_{62} & c_{63} & c_{66} & & \\ c_{41} & c_{42} & c_{43} & c_{46} & c_{44} & \\ c_{51} & c_{52} & c_{53} & c_{56} & c_{54} & c_{55} \end{bmatrix} \end{array} \qquad (19)[15]$$

In this research, the piezoelectric material used is PZT-5H and is modeled in ANSYS using a 3-D coupled field solid element called solid5. The material properties and specifications of PZT-5H are shown in Table 5.

Table 5 Parameters of PHZ-5H

PZT-5H Specification	Unit	Value
s_{11}	M^2 / N	16.5E-12
s_{12}	M^2 / N	-4.78E-12
s_{13}	M^2 / N	-8.45E-12
s_{33}	M^2 / N	20.7E-12
s_{44}	M^2 / N	43.5E-12

Table 5 - *Continued*

s_{66}	M^2 / N	40.56E-12
d_{15}	C / N	7.41E-10
d_{31}	C / N	-2.74E-10
d_{33}	C / N	5.93E-10
K_{11}		3130
K_{33}		3400
ρ	kg / m^3	7500
υ		0.3

The material presented in Appendix A shows a sample ANSYS code and the parameters initialization for ANSYS.

CHAPTER 3

MODELING DESIGN AND OPTIMIZATION

In this Chapter, the fundamental component of the internally leveraged concept (Fig. 7) which is a mono beam will be utilized and analyzed using ANSYS. Then, the simulated performance for various design configurations will be compared relative to applied voltage.

A basic piezoelectric model such as mono beam will be first analyzed to understand the basic properties of piezoelectric material and verify the modeling and simulation procedures. Subsequently, different models will be discussed relative to the applied voltage in an effort to increase the deformation and reduce the stress, how the deformation will be affected by rotating polarization, and what kind of geometry is the best one based on the parameters considered.

The piezoelectric material is PZT-5H and its properties are shown in Table 5. Piezo materials are brittle so the 1st principal stress will be monitored and used in ANSYS. A stress limit of 60MPa is defined to prevent the structure from breaking.

3.1 Mono Beam

The mono beam is the basic model of piezoelectric actuator, and by discussing the four different effects, voltaic effect, gravitational effect, dimensional effect, and polarization effect, the concepts of the piezoelectric ceramics will be developed.

3.1.1 Voltaic Effect

The modeling concept and FEM result are shown in Fig. 10 and Fig. 11. The model is a simple illustration with dimensions, polarization (along x-direction), boundary conditions (fixed button part in x-direction and without gravity effect), and applied voltage. The dimensions are fixed at length (7500 um), thickness (500 um), and depth (500 um). The applied voltage direction is along the polarization direction. By changing the applied voltage, the relationship between max stress, voltage, and deformation could be analyzed.

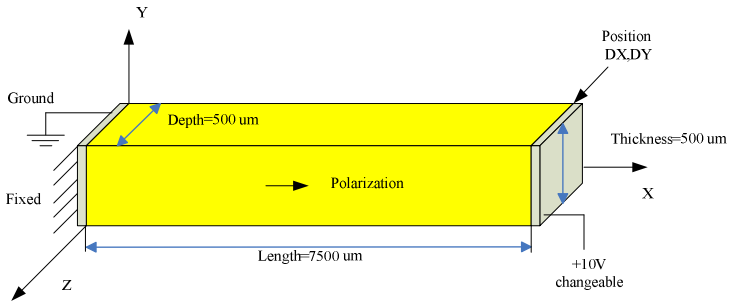

Fig. 10 Scheme about the mono beam applied voltage

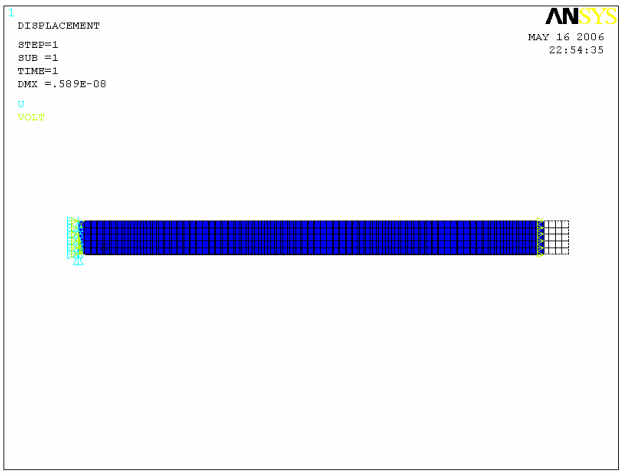

Fig. 11 Simulation for mono beam in ANSYS

Table 6 FEM Results by Changing Applied Voltage

VOLT	DX(M)	DY(M)	STRESS(Pa)
1	-5.89E-10	9.11E-12	1495
2	-1.18E-09	1.82E-11	2990
5	-2.94E-09	4.55E-11	7475
10	-5.89E-09	9.11E-11	14950
20	-1.18E-08	1.82E-10	29901
30	-1.77E-08	2.73E-10	44851
40	-2.35E-08	3.64E-10	59801
50	-2.94E-08	4.55E-10	74751

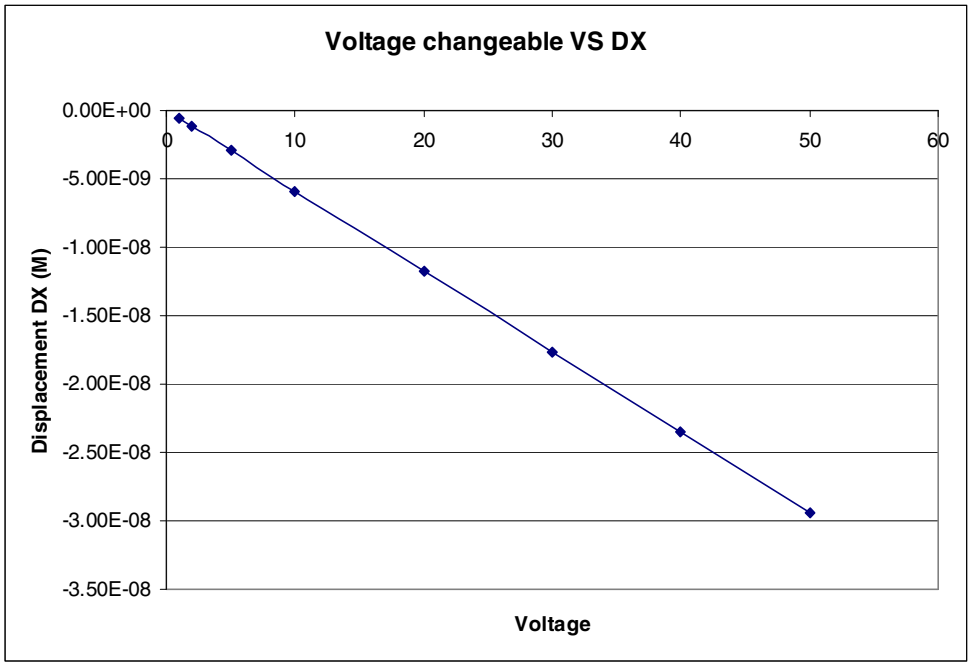

Fig. 12 Displacement sensitivity to voltage changes in X-direction

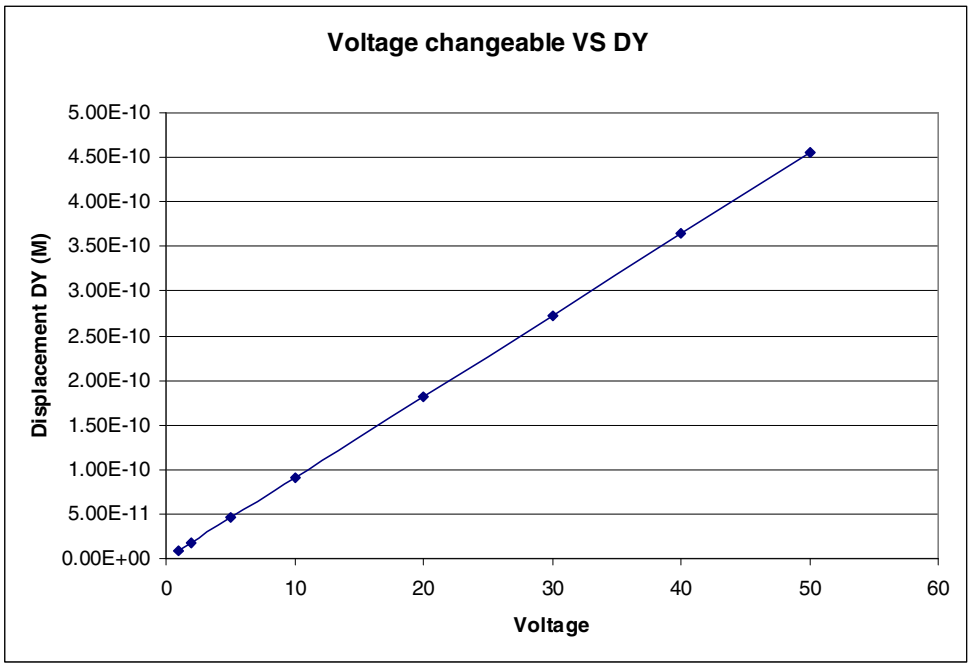

Fig. 13 Displacement sensitivity to voltage changes in Y-direction

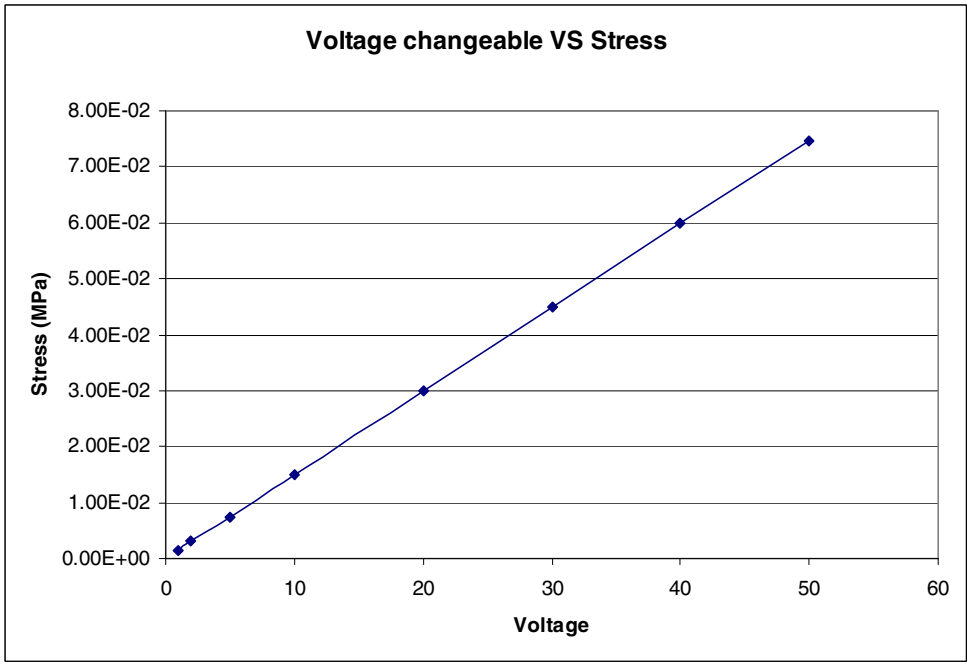

Fig. 14 Stress sensitivity to voltage changes

From Table 6 and graphs (Fig. 12-14), it is observed that when the applied voltage is increasing, DX, DY, and Stress exhibit a linear change. It is one of the basic properties of piezoelectric ceramics.

3.1.2 Gravitational Effect

In this case (Fig. 15), when considering the effect of gravity in Z-direction, there are three cases: (1) with gravitational effect and without voltaic effect, (2) without gravitational effect and with voltaic effect, and (3) with gravitational effect and voltaic effect. These cases will be discussed by changing the depth (in Z-Axis) of the piezoelectric mono beam. All the parameters for length, thickness, material, and polarization (X-direction) remain the same as those in section 3.1.1 with the applied voltage set at 10 V. The mono beam dimensions are length (7500 um), thickness (500 um) while the depth is changed from 50 um to 300 um.

The deformation DX and DY and stress with gravitational effect and without voltaic effect are presented in Table 7. The deformation DX and DY and stress without gravitational effect and with voltaic effect are presented in Table 8. The deformation DX and DY and stress with gravitational effect and with voltaic effect are presented in Table 9.

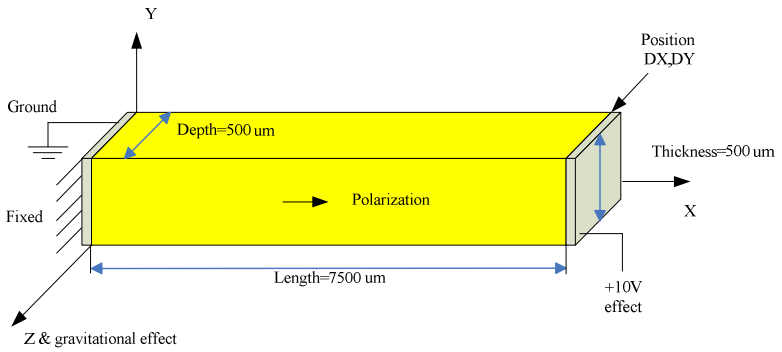

Fig. 15 Illustration of mono beam with voltage and gravity

Table 7 Changing Beam's Depth with Gravitational Effect & without Voltaic Effect

DEPTH(M)	DX(M)	DY(M)	STRESS(MPa)
5.00E-05	1.26E-08	-5.71E-13	3.20E-01
1.00E-04	6.33E-09	-2.40E-13	1.60E-01
1.50E-04	4.21E-09	-1.26E-13	9.70E-02
2.00E-04	3.16E-09	-7.50E-14	7.50E-02
2.50E-04	2.53E-09	-4.30E-14	6.00E-02
3.00E-04	2.11E-09	-2.60E-14	5.20E-02
3.50E-04	1.81E-09	-1.43E-14	4.50E-02
4.00E-04	1.58E-09	-7.16E-15	4.00E-02
4.50E-04	1.41E-09	-1.92E-15	3.60E-02
5.00E-04	1.26E-09	1.64E-15	3.30E-02

Table 8 Changing Beam's Depth without Gravitational Effect and with Voltaic Effect

DEPTH(M)	DX(M)	DY(M)	STRESS(MPa)
5.00E-05	-5.90E-09	9.11E-11	1.90E-02
1.00E-04	-5.90E-09	9.11E-11	1.90E-02
1.50E-04	-5.90E-09	9.11E-11	1.50E-02
2.00E-04	-5.90E-09	9.11E-11	1.40E-02
2.50E-04	-5.89E-09	9.11E-11	1.50E-02
3.00E-04	-5.89E-09	9.11E-11	1.39E-02
3.50E-04	-5.89E-09	9.11E-11	1.50E-02
4.00E-04	-5.89E-09	9.11E-11	1.44E-02
4.50E-04	-5.89E-09	9.11E-11	1.50E-02
5.00E-04	-5.90E-09	9.11E-11	1.90E-02

Table 9 Changing Beam's Depth with Gravitational Effect and with Voltaic Effect

DEPTH(M)	DX(M)	DY(M)	STRESS(MPa)
5.00E-05	6.73E-09	9.06E-11	3.31E-01
1.00E-04	4.33E-10	9.09E-11	1.69E-01
1.50E-04	-1.69E-09	9.10E-11	9.61E-02
2.00E-04	-2.73E-09	9.10E-11	6.86E-02
2.50E-04	-3.36E-09	9.11E-11	5.44E-02
3.00E-04	-3.78E-09	9.11E-11	4.60E-02
3.50E-04	-4.08E-09	9.11E-11	4.23E-02
4.00E-04	-4.31E-09	9.11E-11	3.79E-02
4.50E-04	-4.48E-09	9.11E-11	3.56E-02
5.00E-04	-4.62E-09	9.11E-11	3.27E-02

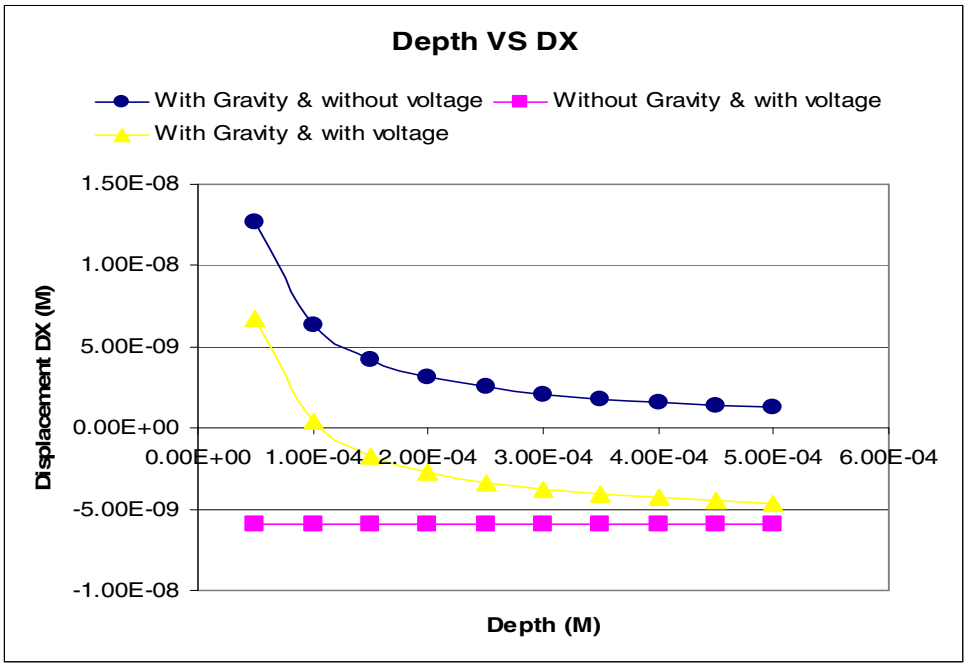

Fig. 16 Displacement sensitivity to depth in X-direction by different situations

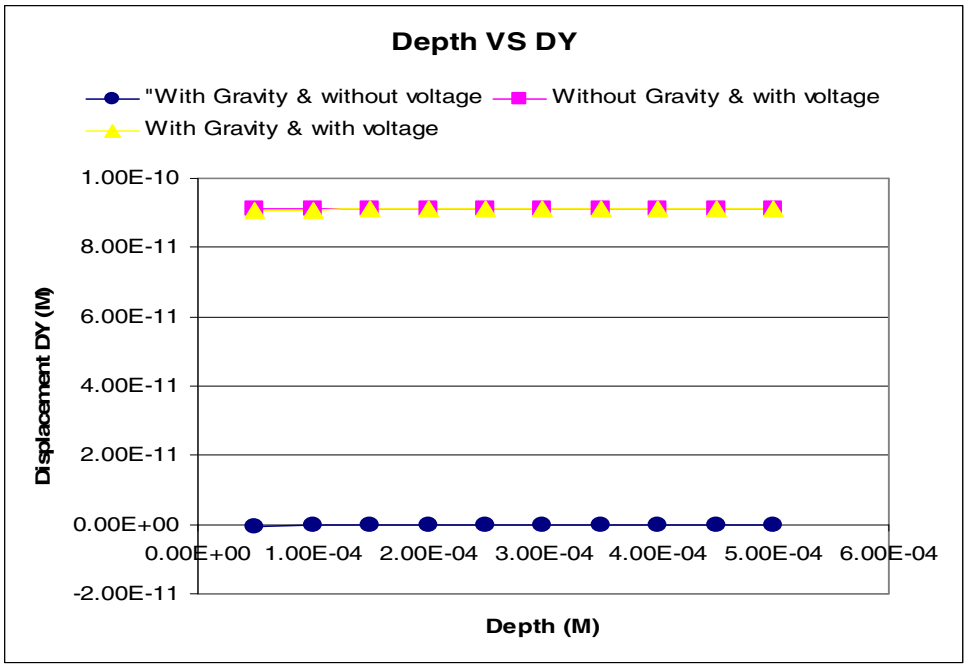

Fig. 17 Displacement sensitivity to depth in X-direction for all cases

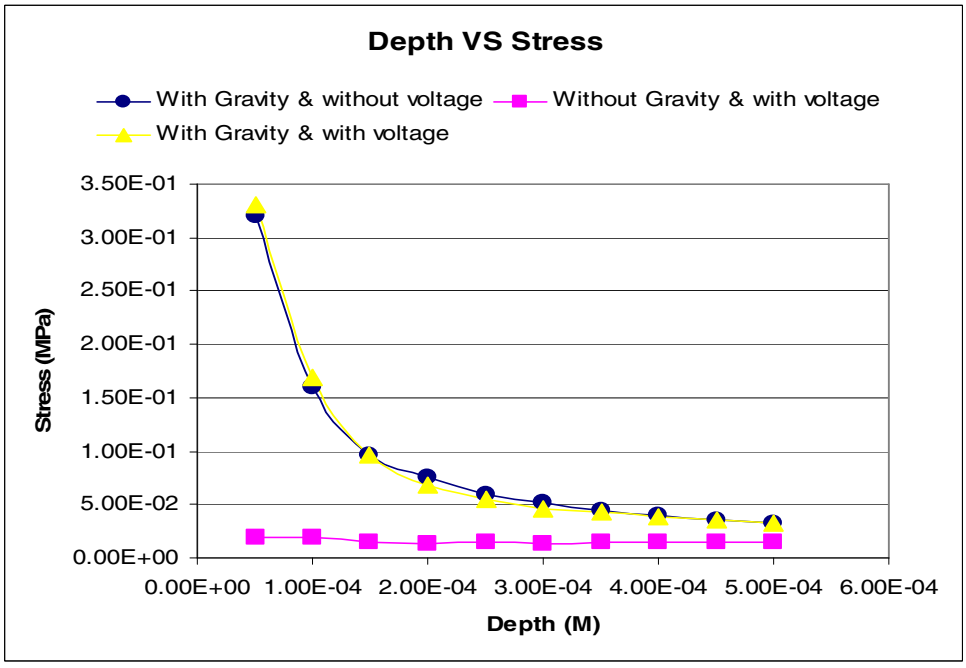

Fig. 18 Stress sensitivity to depth for all cases

From Fig. (15-18), and Tables (7-9), at first, to see the blue line with circle (with gravity effect and without voltaic effect), when depth is larger, the effect of the gravity will become smaller. The red line with square, without gravity effect and with voltaic effect, does not change and keeps the same value. From the yellow line with triangle, it is applied the voltage and has the gravity effect. The results, displacement and stress, combined by blue and red lines are equal to the results from yellow line indicating that the gravity effect and voltage are independent. It means that in the same dimensions, when the applied voltage is increasing, the displacement from voltage effect will increase, and the displacement form gravity will be the same. When the applied voltage is larger, the effect by the gravity will become smaller.

3.1.3 Dimensional Effect

The results from section 3.1.2 (gravitational effects) indicate that the gravitational effect and voltaic effect are independent. So, to simplify the analysis, the gravitational effect will be ignored and the same voltage will be applied on the electrodes as shown in Fig. 19, and the dimensions in x, y, or z-direction would be modified to in order to observe their effect on stress and displacement.

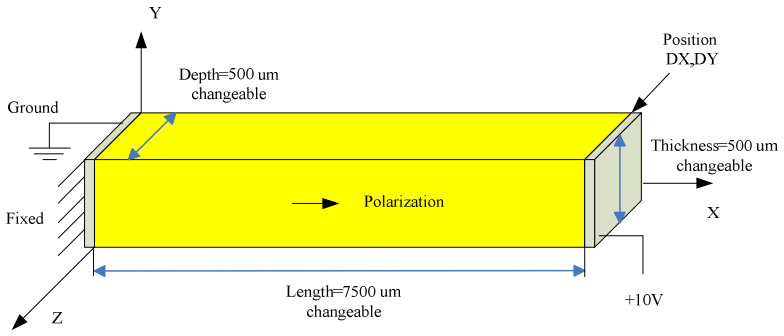

Fig. 19 Scheme for piezoelectric beam by dimensional effect

Three cases will be discussed; (1) changing length, (2) changing thickness, and (3) changing depth. The results from the first case, changing length from 1000 um to 8000 um are presented in Figures (19-22) and Table 10. It is observed that there is a nonlinear relationship between the displacement in X-direction and the length.

Table 10 Deformations by Changing Beam Length

LENGTH(M)	DX(M)	DY(M)	STRESS(MPa)
1.00E-03	-5.61E-09	6.70E-10	1.10E-01
2.00E-03	-5.77E-09	3.39E-10	5.56E-02
3.00E-03	-5.82E-09	2.27E-10	3.72E-02
4.00E-03	-5.85E-09	1.70E-10	2.80E-02
5.00E-03	-5.86E-09	1.36E-10	2.24E-02
6.00E-03	-5.87E-09	1.14E-10	1.87E-02
7.00E-03	-5.88E-09	9.75E-11	1.60E-02
8.00E-03	-5.89E-09	8.54E-11	1.40E-02

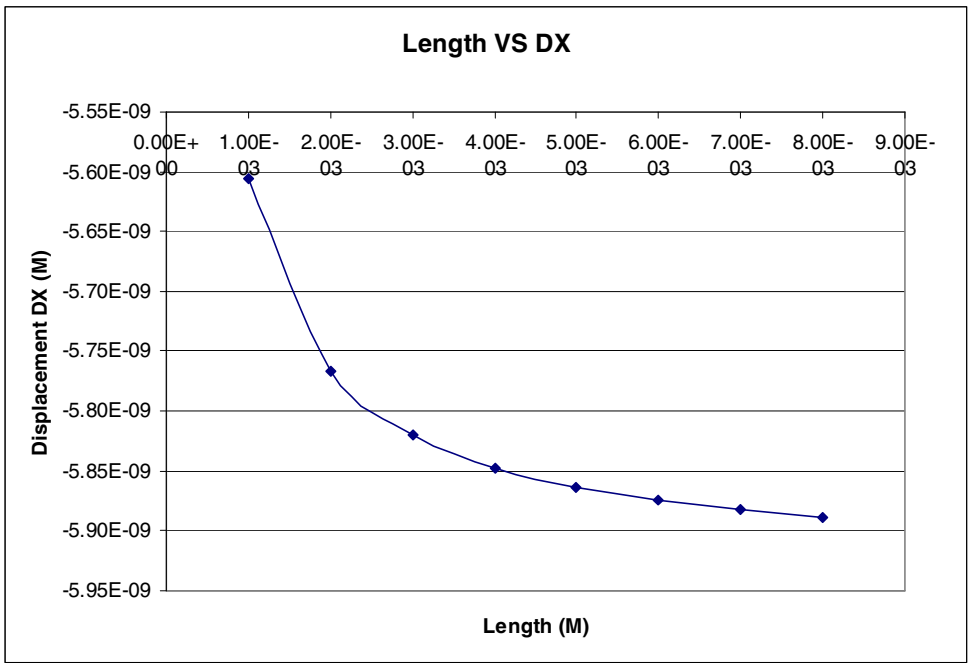

Fig. 20 Displacement sensitivity to beam length in X-direction

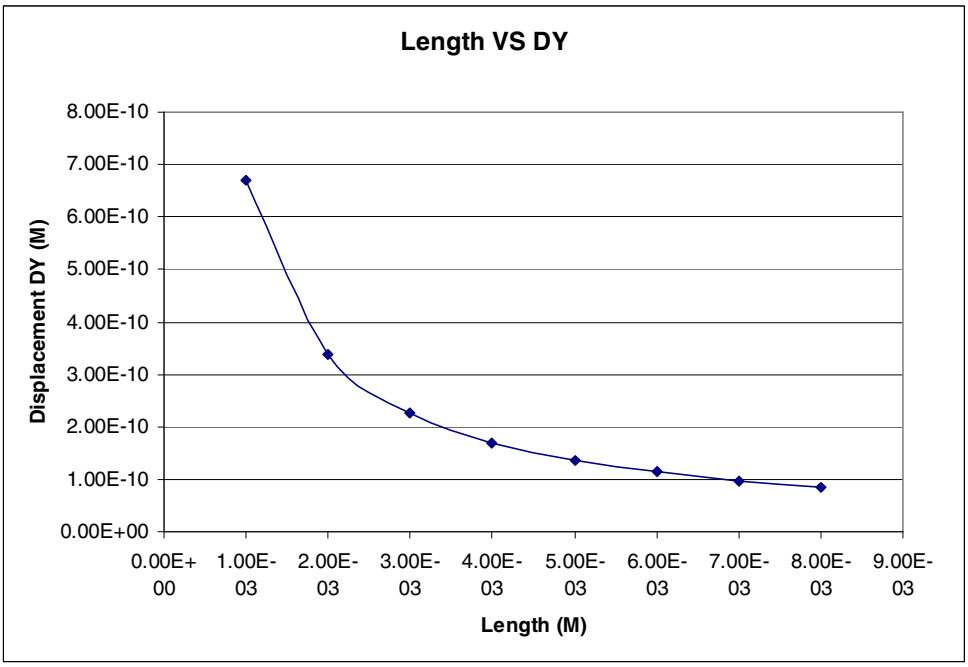

Fig. 21 Displacement sensitivity to beam length in Y-direction

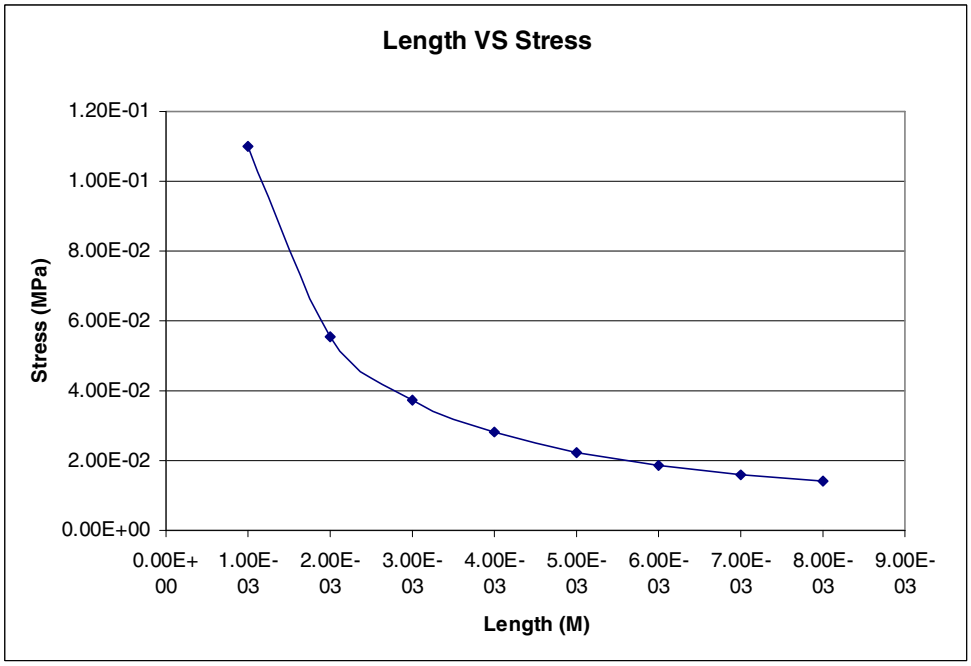

Fig. 22 Stress sensitivity to beam length

By changing the dimensions from 100 um to 500 um in the y-direction (thickness) and z-direction (depth) independently, Tables (11-12) and Figures (23-28) are obtained. When the changing dimensions are not along the polarization direction the absolute results in y-direction (thickness) and z-direction (depth) remain the same.

Table 11 Deformations by Changing Beam Thickness

THICKNESS(M)	DX(M)	DY(M)	STRESS(MPa)
1.00E-04	-5.90E-09	1.82E-11	1.90E-02
2.00E-04	-5.90E-09	3.65E-11	1.40E-02
3.00E-04	-5.89E-09	5.47E-11	1.39E-02
4.00E-04	-5.89E-09	7.29E-11	1.45E-02
5.00E-04	-5.89E-09	9.11E-11	1.50E-02

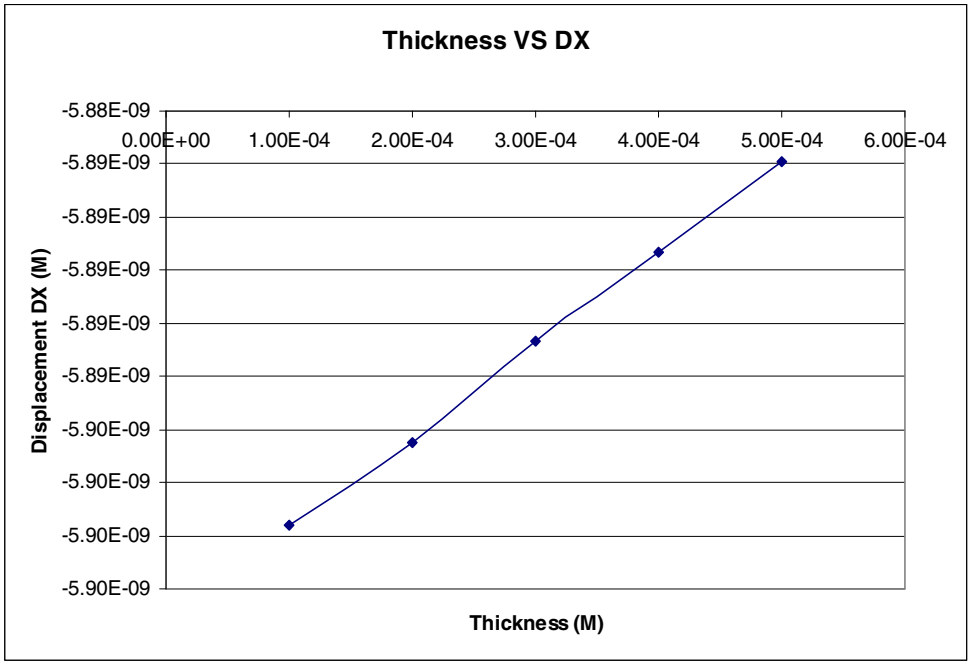

Fig. 23 Displacement sensitivity to beam thickness in X-direction

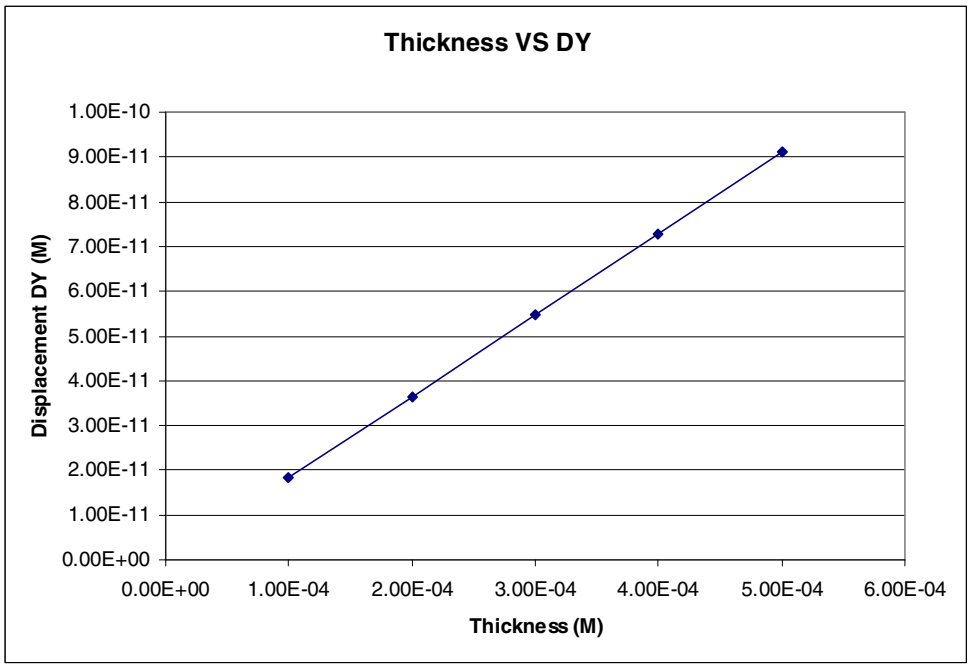

Fig. 24 Displacement sensitivity to beam thickness in Y-direction

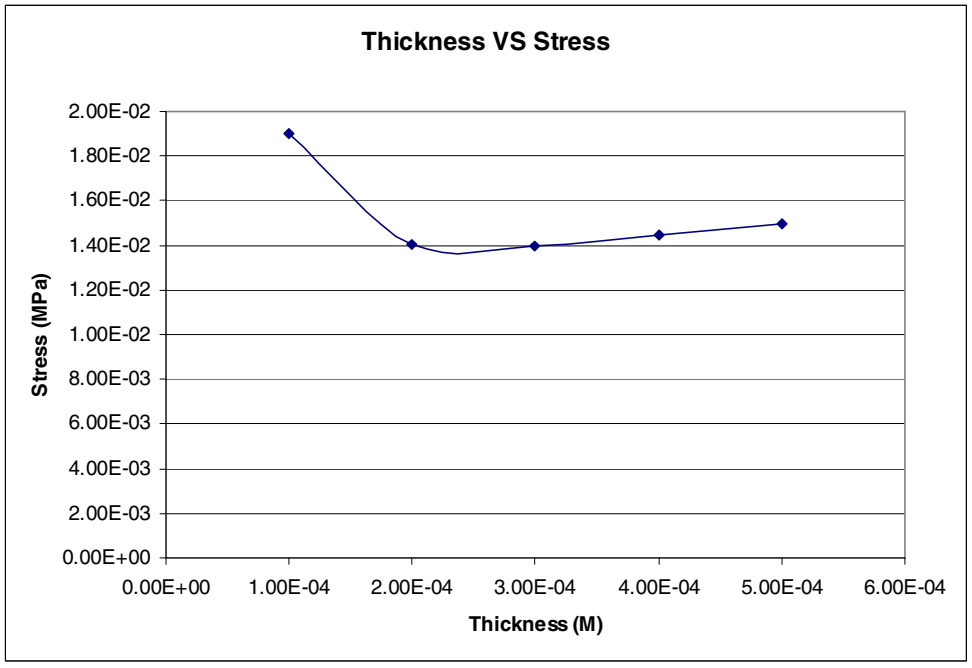

Fig. 25 Stress sensitivity to beam thickness

Table 12 Deformations by Changing Beam Depth

DEPTH(M)	DX(M)	DY(M)	STRESS(MPa)
1.00E-04	-5.90E-09	9.11E-11	1.90E-02
2.00E-04	-5.90E-09	9.11E-11	1.40E-02
3.00E-04	-5.89E-09	9.11E-11	1.39E-02
4.00E-04	-5.89E-09	9.11E-11	1.45E-02
5.00E-04	-5.89E-09	9.11E-11	1.50E-02

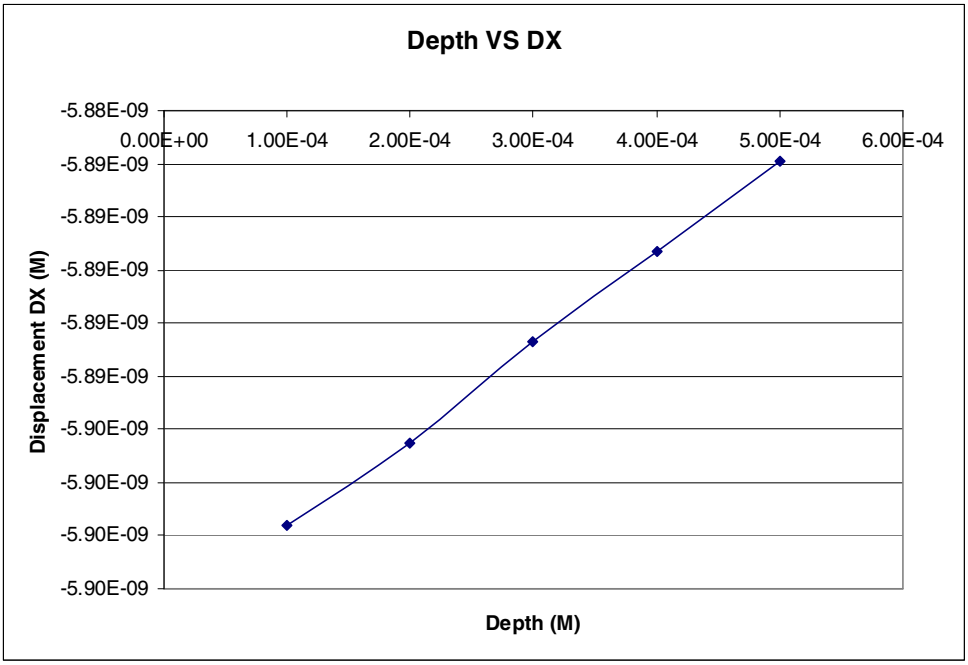

Fig. 26 Displacement sensitivity to beam depth in X-direction

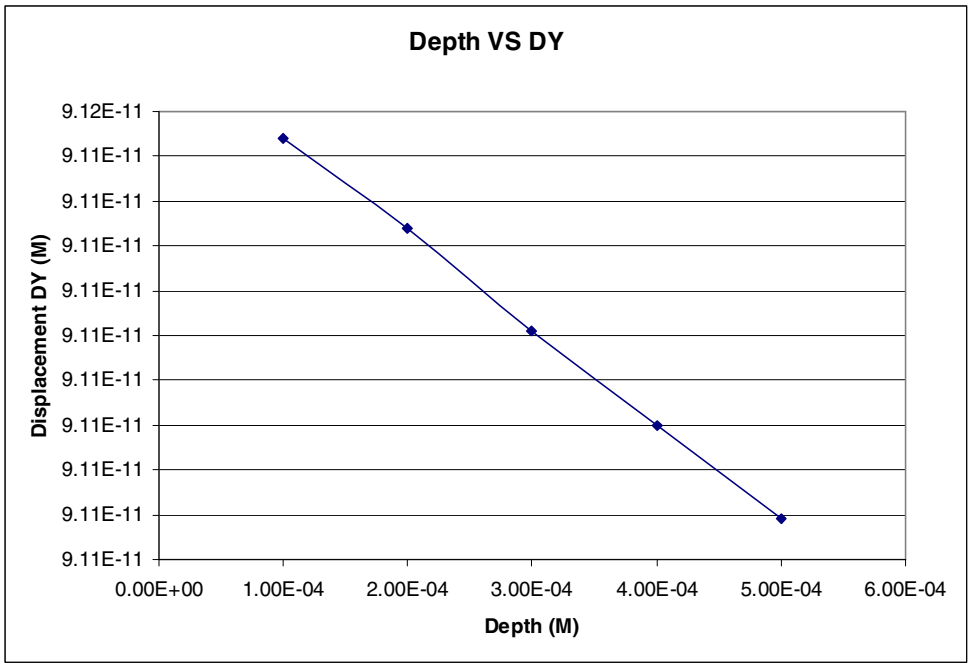

Fig. 27 Displacement sensitivity to beam depth in Y-direction

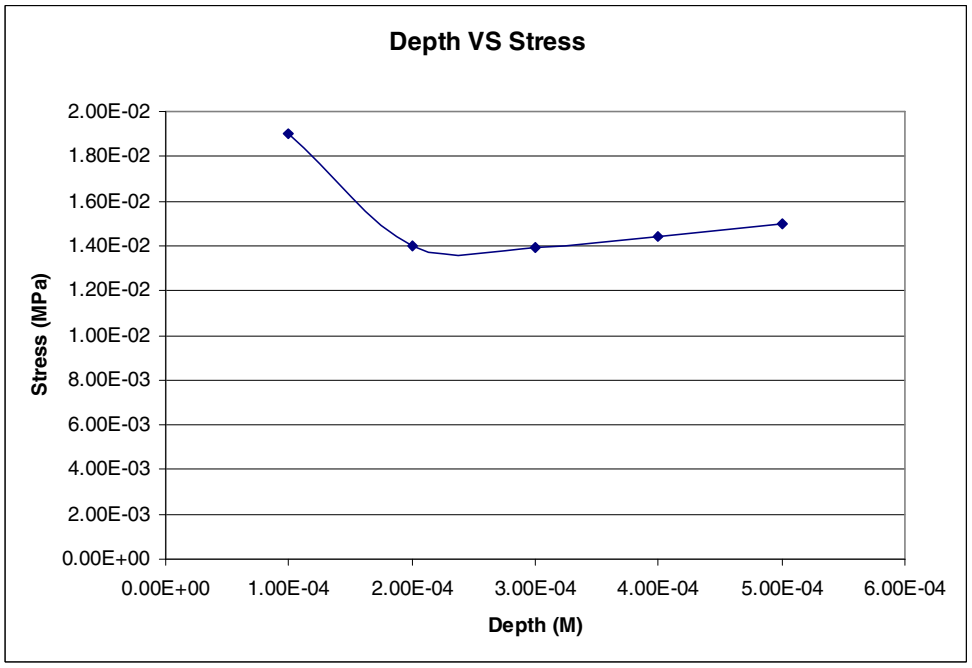

Fig. 28 Stress sensitivity to beam depth

3.1.4 Polarization Effect

Originally, the voltage is applied along the polarization direction on the right and left sides of the piezoelectric beam as discussed in section 3.1.1 (Voltaic effect), 3.1.2 (Gravitational effect) and 3.1.3 (Dimensional effect). When the polarization and voltaic directions are the same, the structure will be expanding or contracting. In this section, the effect of polarization direction will be examined when the polarization and voltaic directions are perpendicular to each other with all other parameters remaining the same. The polarization is defined to be along the Y-direction as shown in Fig. 29.

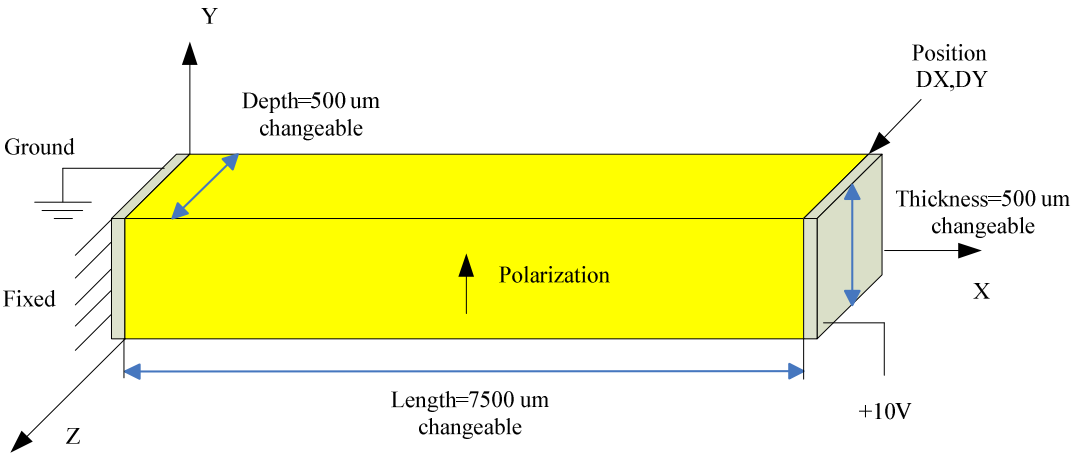

Fig. 29 Polarization effect along Y-direction and voltaic effect along X-direction

When the applied voltage is along the polarization direction the structure will be contracting or expanding. However, when the polarization direction rotates 90 degrees (from X-direction to Y-direction), the structure exhibits a bending behavior as shown in Fig. 30.

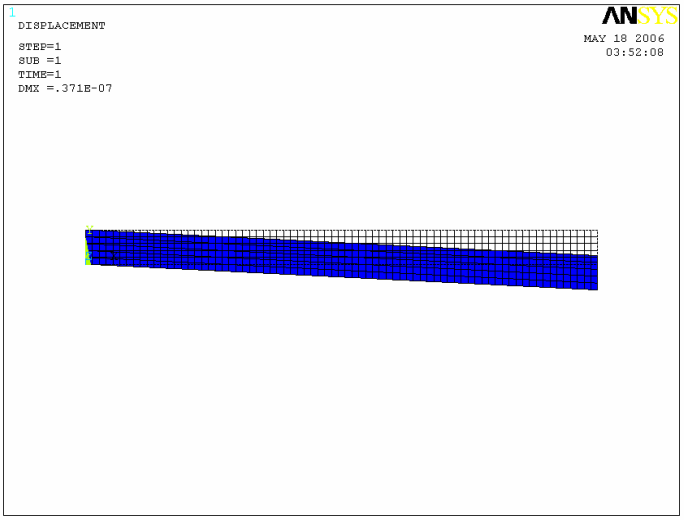

Fig. 30 Simulation for mono beam in ANSYS with polarization along Y-direction and voltaic effect along X-direction

In this section all the parameters and conditions remain the same as those before, but the voltaic direction is modified to be perpendicular to the voltaic direction as shown in Fig. 31. The behavior of the beam is also bending as shown in Fig. 32. So, when the voltaic effect and polarization directions are parallel, the piezo will be expanding or contracting. On the other hand, when the voltaic effect and polarization directions are crossed, the piezo will exhibit a bending behavior. Therefore, by defining the polarization and voltaic directions of the beam, the behavior of the beam can be predicted.

Four typical types for the mono beam relative to polarization and voltaic directions are presented for clarity in Figs. 33-36.

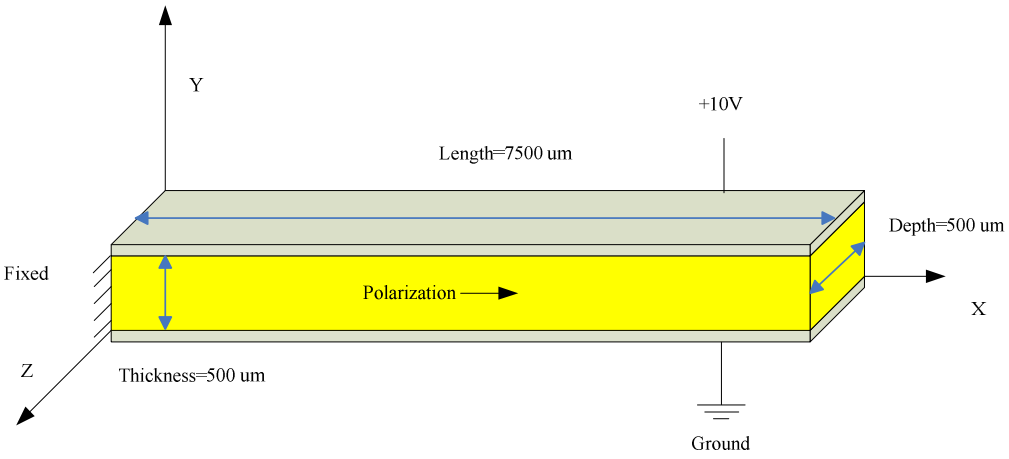

Fig. 31 Polarization along X-direction and voltaic effect along Y-direction

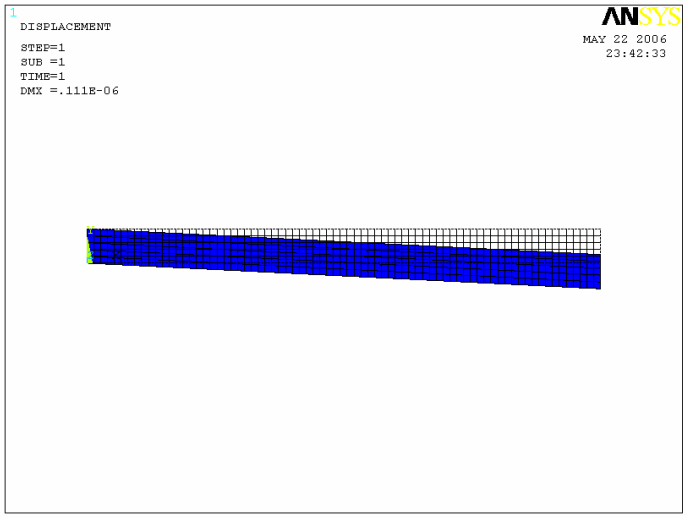

Fig. 32 Simulation for mono beam in ANSYS and voltaic direction along Y-direction

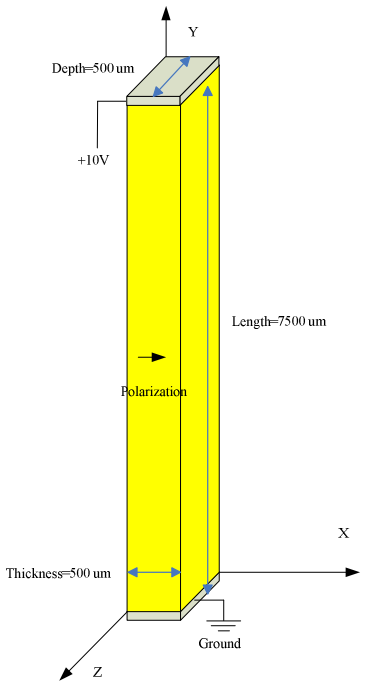

(a)

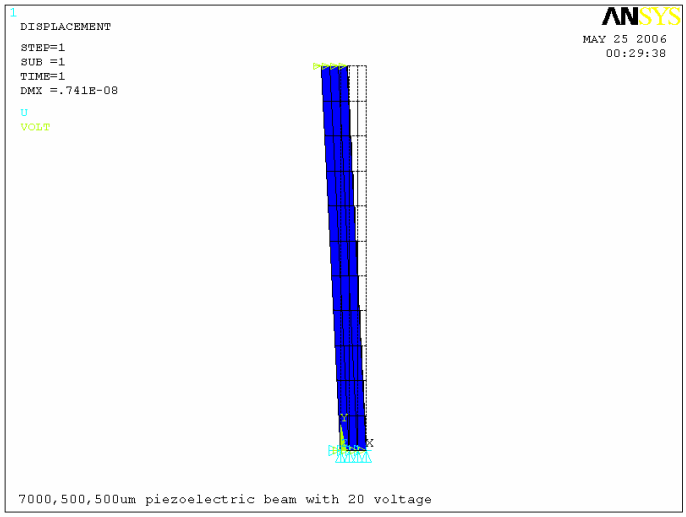

(b)

Fig. 33 Beam geometry (a) simulation (b) X-Axis polarization and Y-Axis voltaic direction (bending)

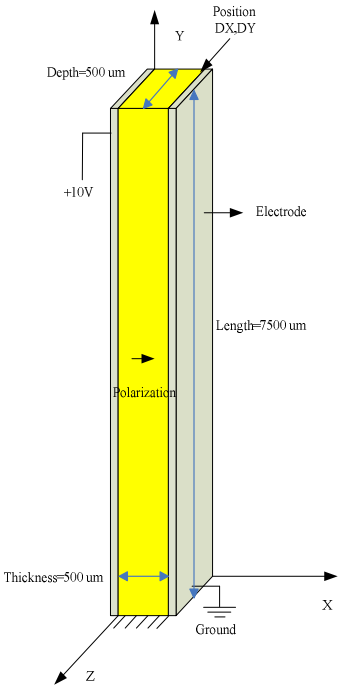

(a)

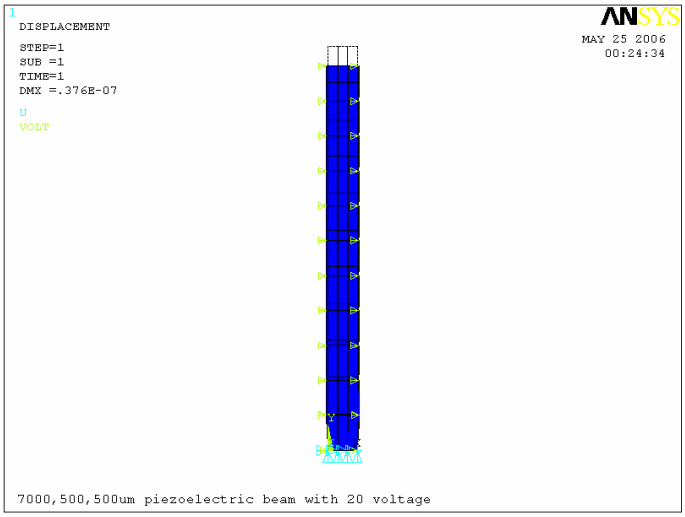

(b)

Fig. 34 Beam geometry (a) simulation (b) X-Axis polarization and X-Axis voltaic direction (contraction)

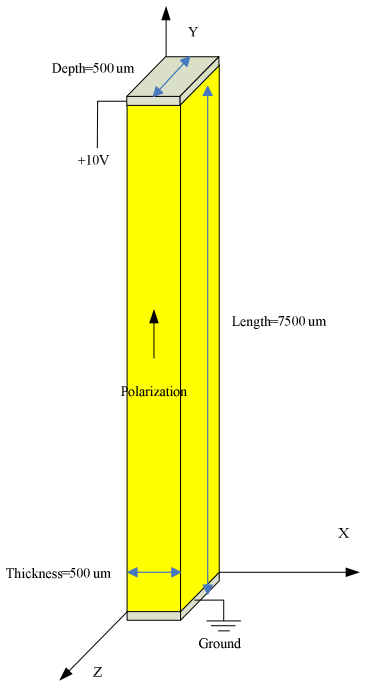

(a)

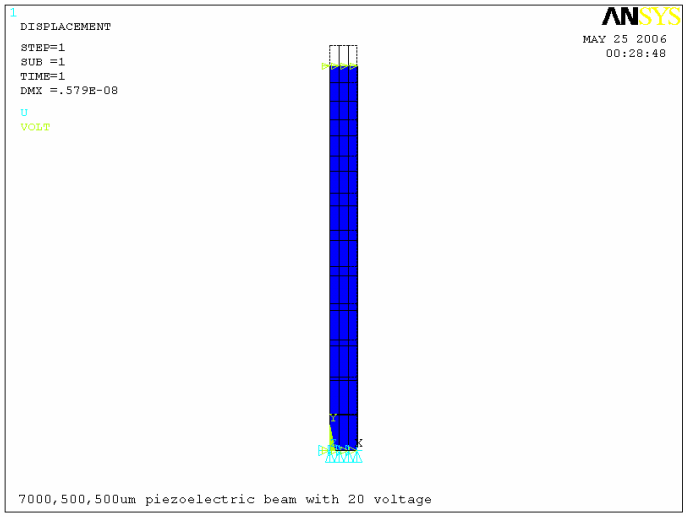

(b)

Fig. 35 Beam geometry (a) and simulation (b) in Y-Axis polarization and Y-Axis voltaic direction (contraction)

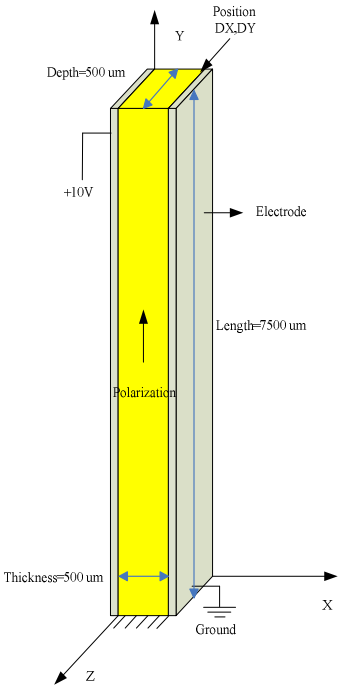

(a)

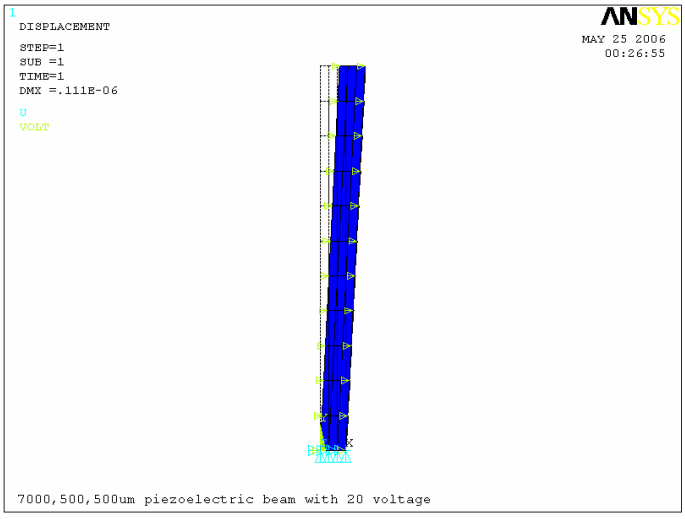

(b)

Fig. 36 Beam geometry (a) simulation (b) Y-Axis polarization and X-Axis voltaic direction (bending)

3.2 Bimorph Beam

The bimorph beam is a very useful, common, and basic way to produce bending moment. The bimorph beam has been studied in the literature [9] and an arrangement is shown in Fig. 37 along with a simulated result in Fig. 38. One of its applications is to amplify the displacement of a piezoelectric actuator. Due to the opposite polarization direction and with the same voltaic direction, the left side of the structure will contract and right side will expand. When combining these two parts, the bimorph beam will generate moment that would amplify the displacement.

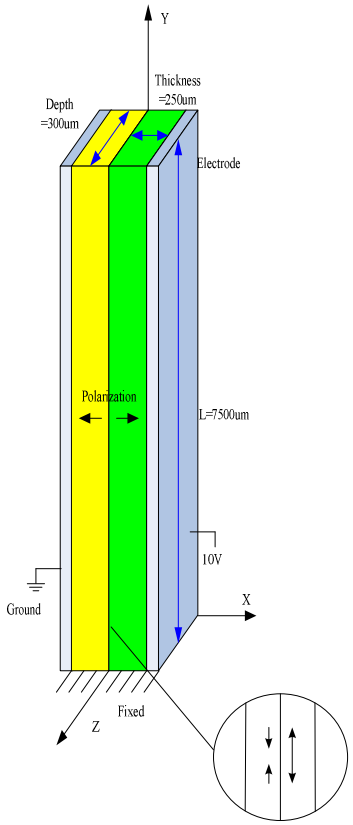

Fig. 37 Scheme of bimorph beam

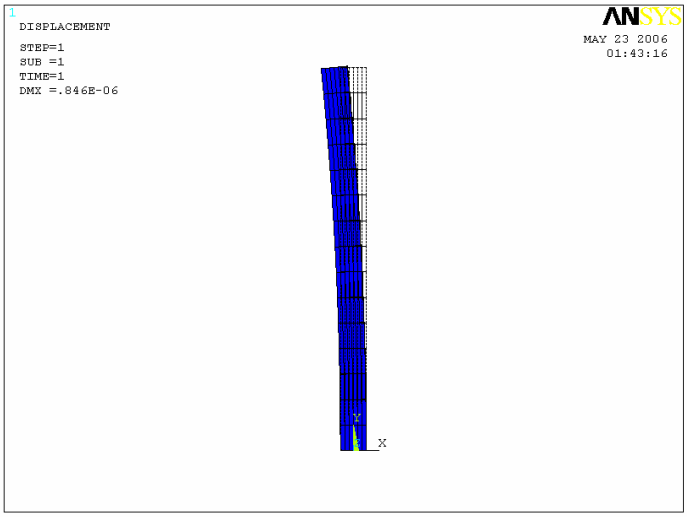

Fig. 38 Simulation of bimorph beam

In this section, the length L (7500 um), and depth (300 um) will be fixed, while the thickness will be changeable. The effect of thickness on the performance of the piezoelectric beam is studied by varying the thickness from 100 um to 500 um and observing the response displacement.

The results are tabulated in Table 13, and plotted in Fig. 39-41. By comparing the results among Fig. 33, Fig. 34 and Fig.38 in the same dimensions, the results are -0.0074 um, -0.0029 um and -1.34 um separately. The way about bimorph beam generates larger displacement than others. To prevent the structure from breakage, the maximum stress of PZT-5H is monitored not to exceed 60 MPa. Another study is performed in which the stress is defined to be 60 MPa in order to explore the influence of thickness on displacement and voltage. The results are shown in Fig. 42 and Fig. 43,

and show that the thinnest beam will produce the maximum displacement with the lower applied voltage.

Table 13 The Deformations by Changing Beam Thickness

THICKNESS(M)	DX(M)	DY(M)	STRESS(MPa)
1.00E-04	-5.28E-06	1.41E-07	1.72E+00
2.00E-04	-1.34E-06	7.09E-08	8.58E-01
3.00E-04	-6.00E-07	4.78E-08	6.21E-01
4.00E-04	-3.40E-07	3.60E-08	5.08E-01
5.00E-04	-2.18E-07	2.88E-08	4.50E-01

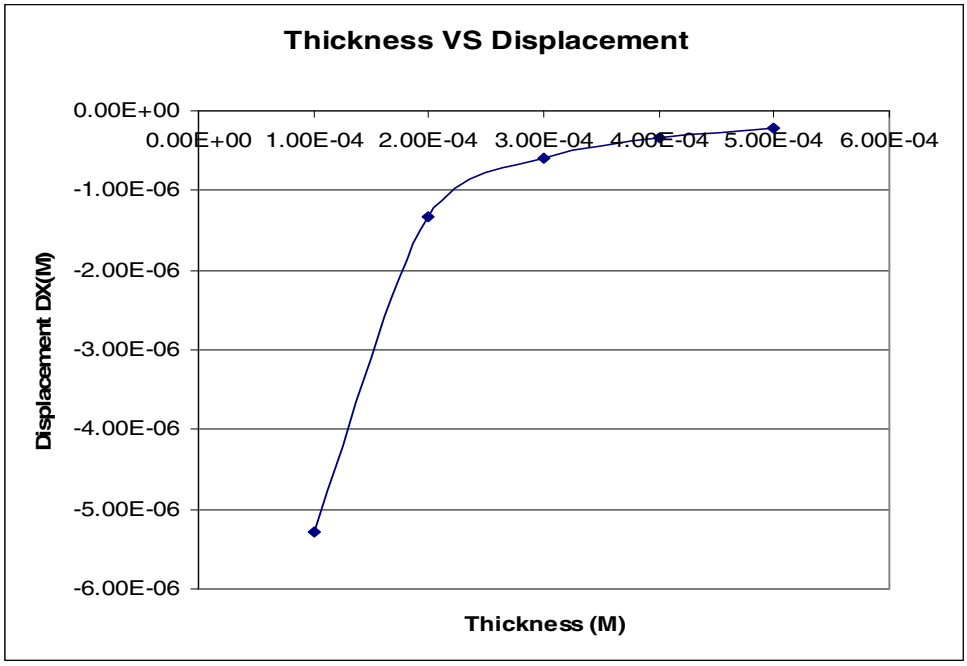

Fig. 39 Displacement sensitivity to thickness in X-direction

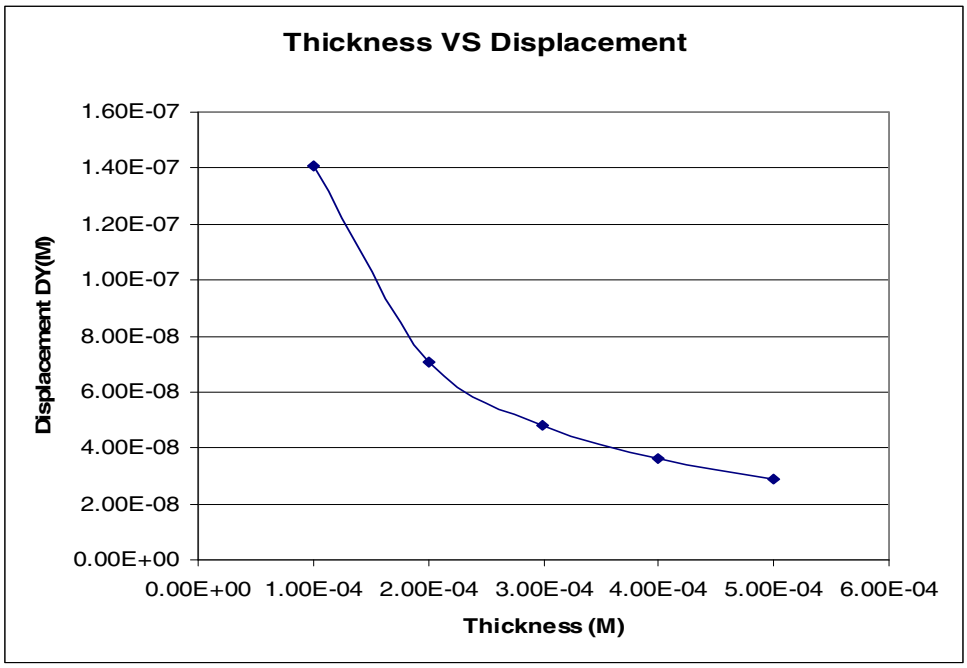

Fig. 40 Displacement sensitivity to thickness in Y-direction

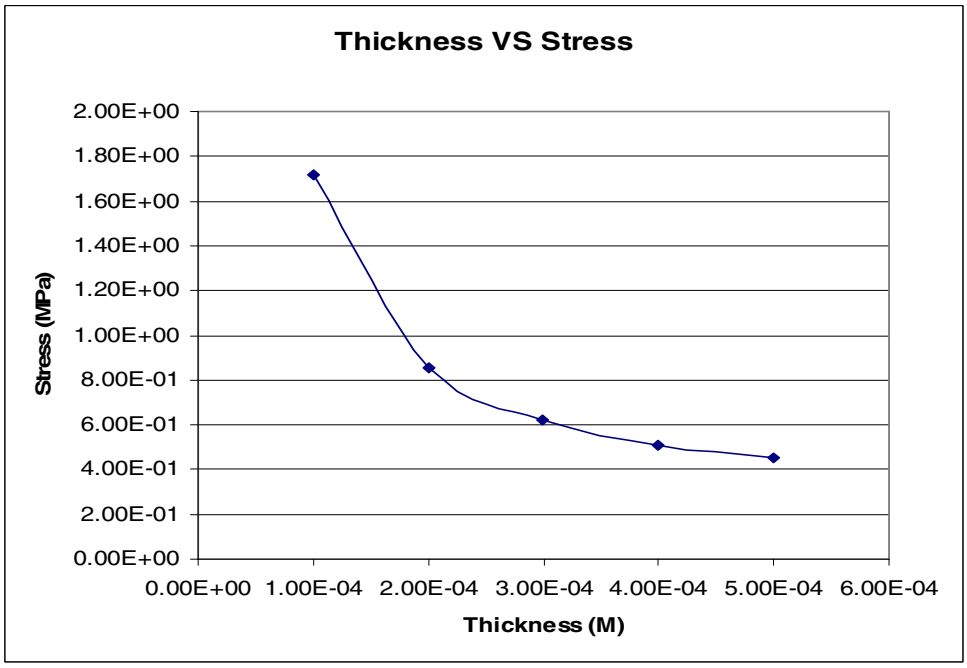

Fig. 41 Stress sensitivity to thickness

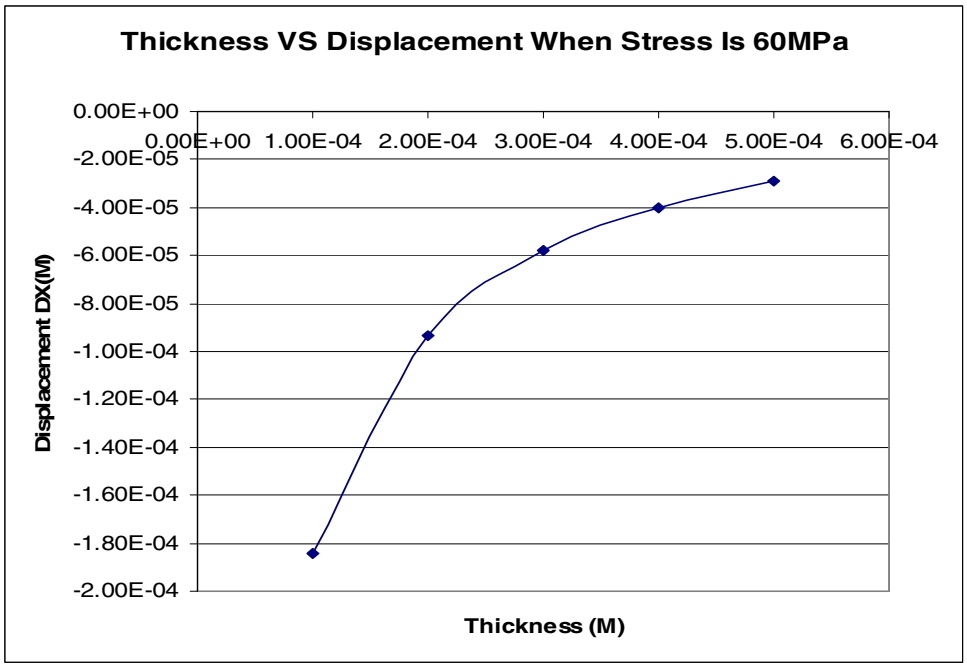

Fig. 42 Displacement sensitivity to thickness in X-direction when stress is 60 MPa

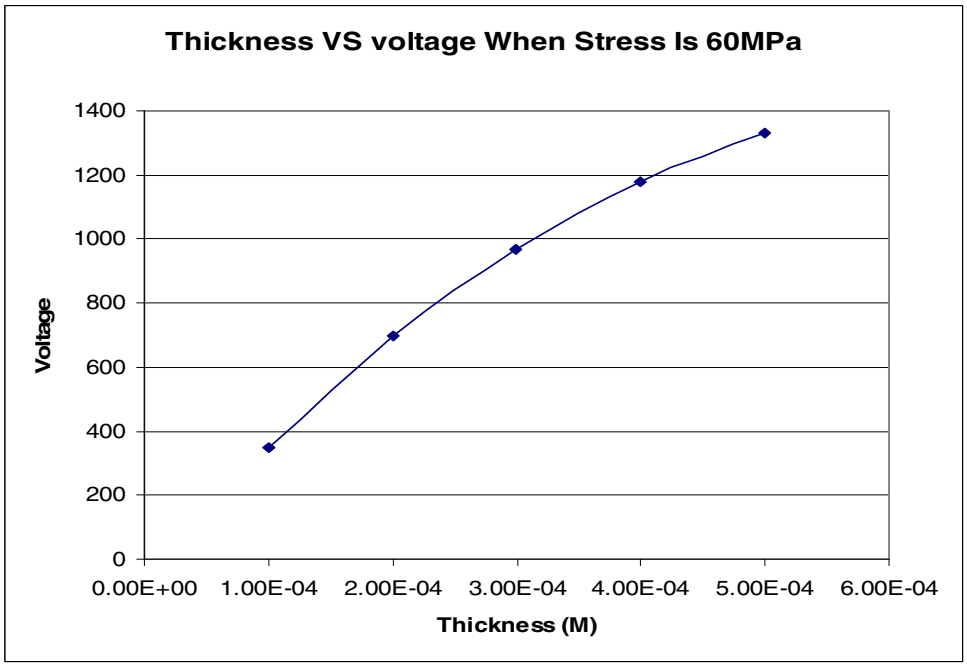

Fig. 43 Voltage sensitivity to thickness when stress is 60 MPa

3.3 Shear Mode

In the mono beam and bimorph beam discussion, the voltage is applied on the entire single side electrode, and the entire opposite side electrode is grounded. In this section, the procedure for generating a shear mode in order to increase the displacement is presented and studied through the changing of various geometric parameters.

The design purpose is to utilize the properties of contraction and expansion by applying different voltaic direction. At first, from the mono beam Fig. 44, it is recognized that L2 will contract, and L1 will expand. When two parts are combined together, the bottom part of the piezoelectric beam will generate moment and rotation due to the inner shear force. Even if the rotation ratio is small, when the piezoelectric beam is long, the tip displacement will be amplified.

Then why it can not be fixed at the button part of the actuator? That is because L2 is contracting and L1 is expanding, the motion of the piezoelectric actuator will still be along the central line as Fig. 45. The effect of the shear mode of the beam will be reduced.

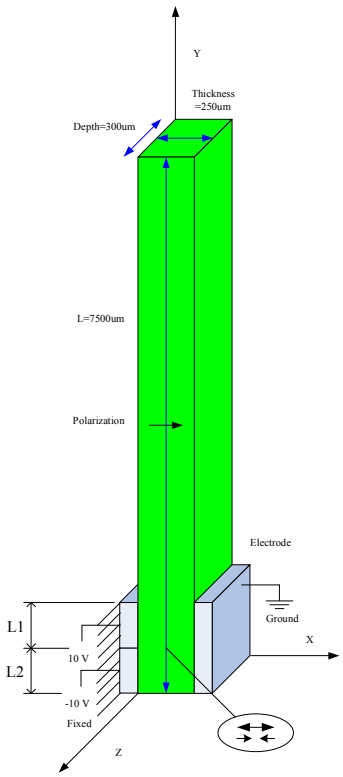

(a)

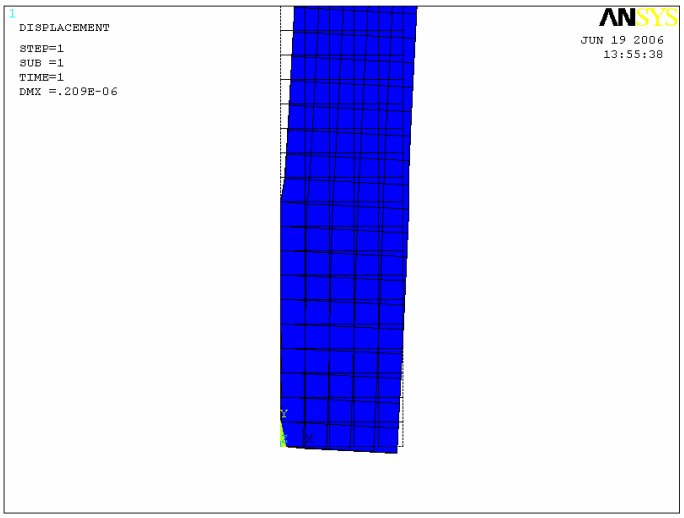

(b)

Fig. 44 Beam in shear mode (a) geometry, (b) response

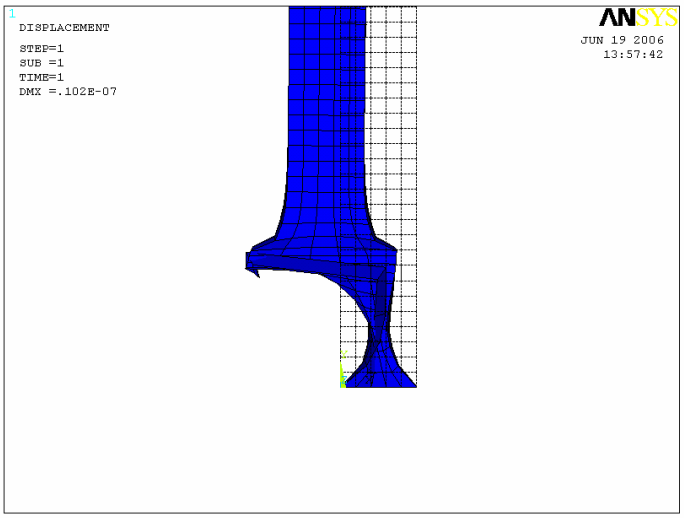

Fig. 45 Simulation of the button part fixed in shear mode

The effect of thickness on the performance of the piezoelectric beam is studied by varying the thickness from 100 um to 500 um and observing the response displacement. From Table 14 and Fig. 46-48, when the thickness is 100 um the displacement and stress are the largest. However, when the thickness is larger than 200 um the displacement increase is not substantial.

In addition, the displacement sensitivity due to L1 (changing from 100 um to 3000 um) is performed with the results presented in Table 15, and plotted in Fig. 49-51. When L1 is 100 um, the displacement in X-direction is the largest and the stress is the smallest. When L1 is larger than 500 um, the changes become smaller.

Table 14 Deformations by Changing the Thickness of the Beam

THICKNESS(M)	DX(M)	DY(M)	STRESS(MPa)
1.00E-04	3.14E-07	-5.88E-09	4.62
1.50E-04	2.34E-07	-6.40E-09	4.58
2.00E-04	2.15E-07	-7.49E-09	4.53
2.50E-04	2.09E-07	-8.75E-09	4.47
3.00E-04	2.06E-07	-1.01E-08	4.45
3.50E-04	2.04E-07	-1.14E-08	4.43
4.00E-04	2.02E-07	-1.27E-08	4.43
4.50E-04	2.01E-07	-1.40E-08	4.42
5.00E-04	2.00E-07	-1.53E-08	4.42

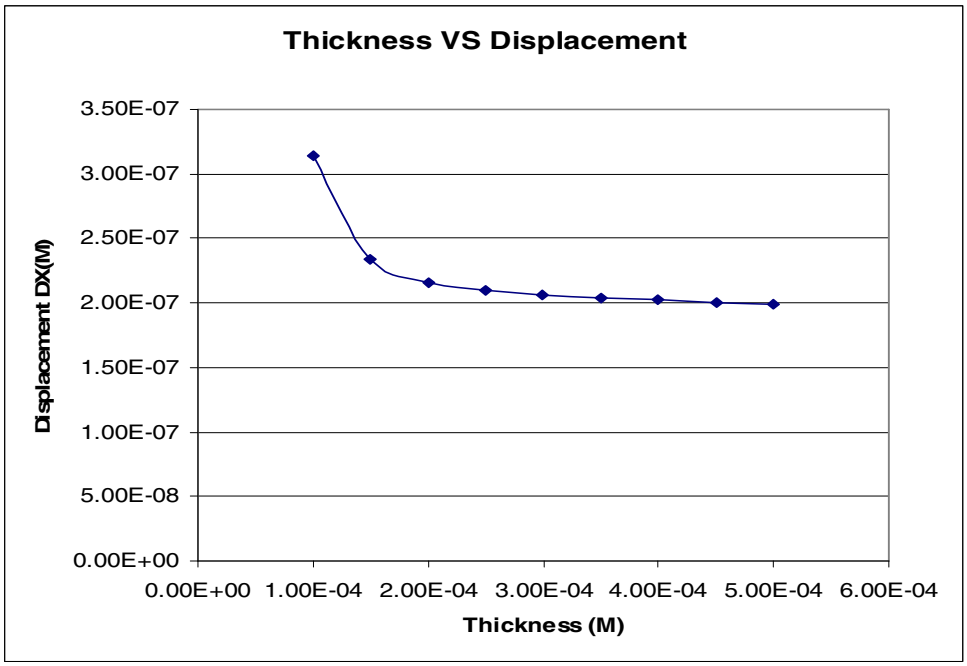

Fig. 46 Displacement sensitivity to thickness in X-direction

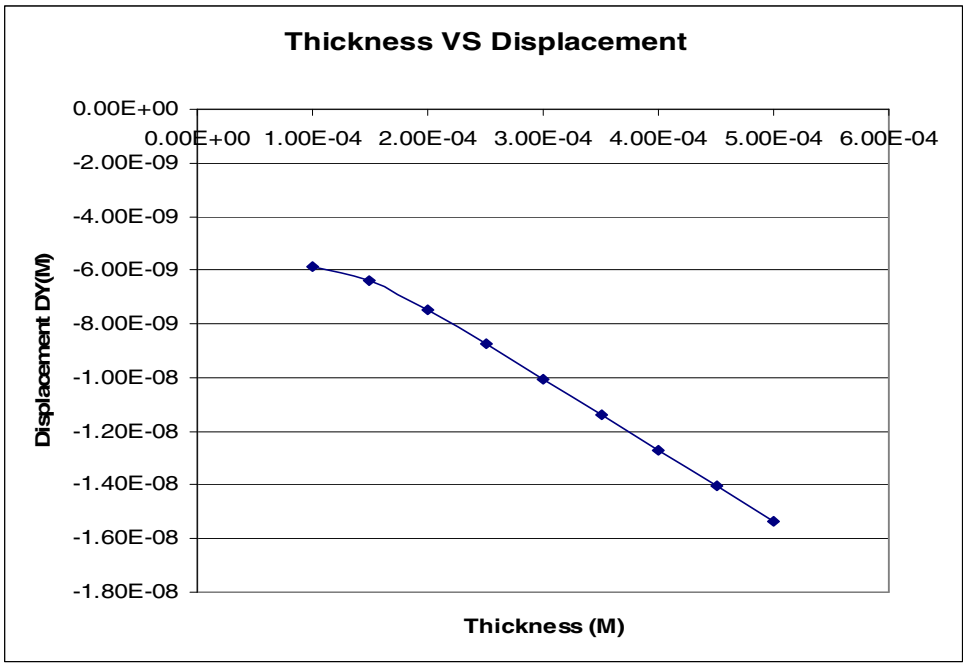

Fig. 47 Displacement sensitivity to thickness in Y-direction

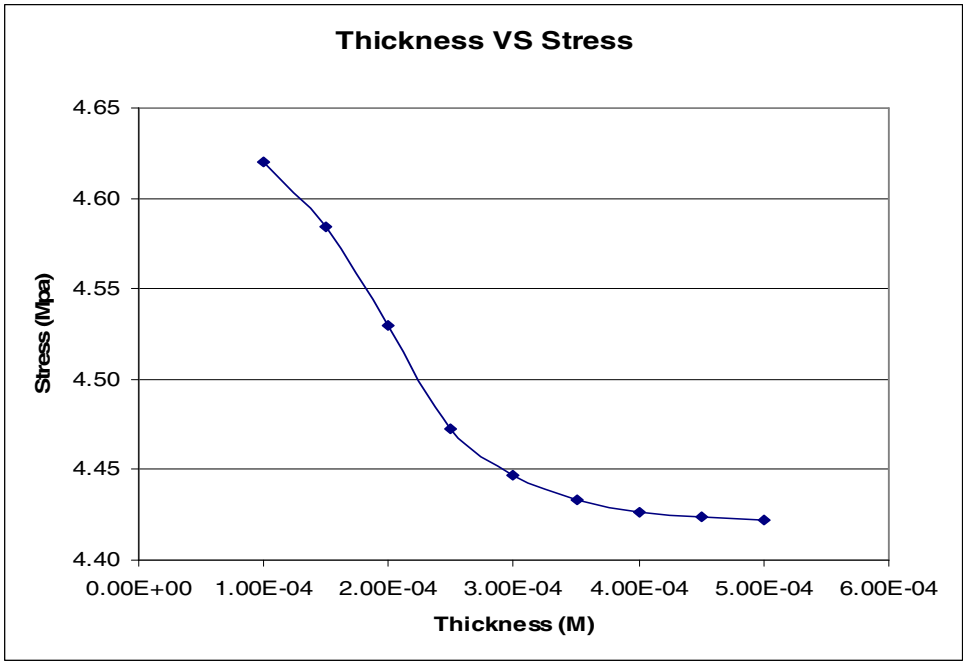

Fig. 48 Stress sensitivity to thickness

Table 15 The Deformations by Changing L1 of the Beam

L1 (M)	DX(M)	DY(M)	STRESS(MPa)
1.00E-04	2.80E-07	-1.09E-08	4.41
2.00E-04	2.33E-07	-9.49E-09	4.43
3.00E-04	1.89E-07	-8.11E-09	4.53
4.00E-04	1.59E-07	-7.13E-09	4.63
5.00E-04	1.40E-07	-6.50E-09	4.70
1.00E-03	1.07E-07	-5.48E-09	4.82
2.00E-03	8.76E-08	-5.32E-09	4.83
3.00E-03	7.15E-08	-5.32E-09	4.84

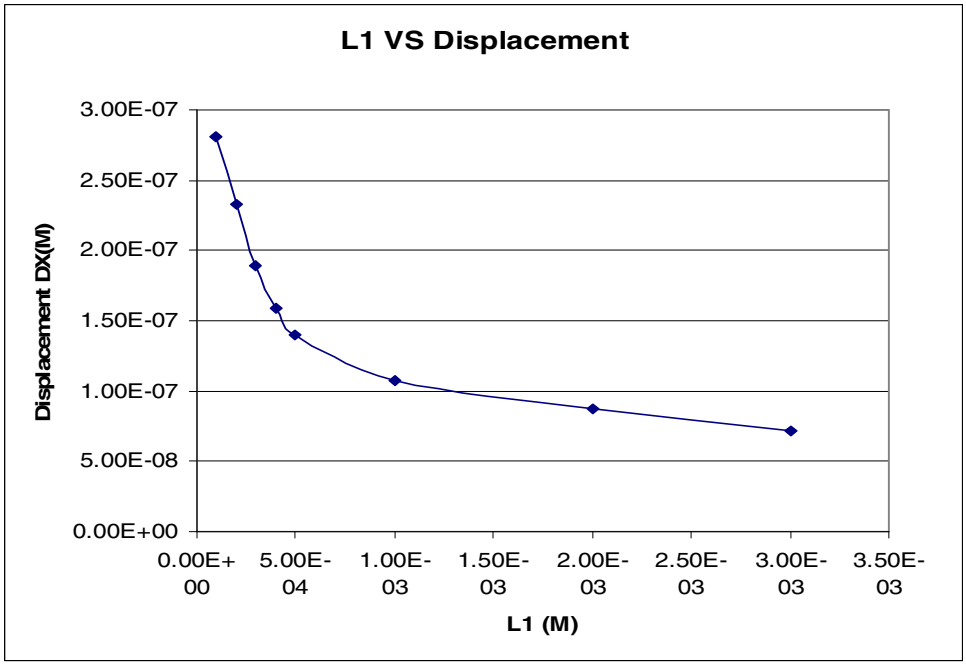

Fig. 49 Displacement sensitivity to L1 in X-direction

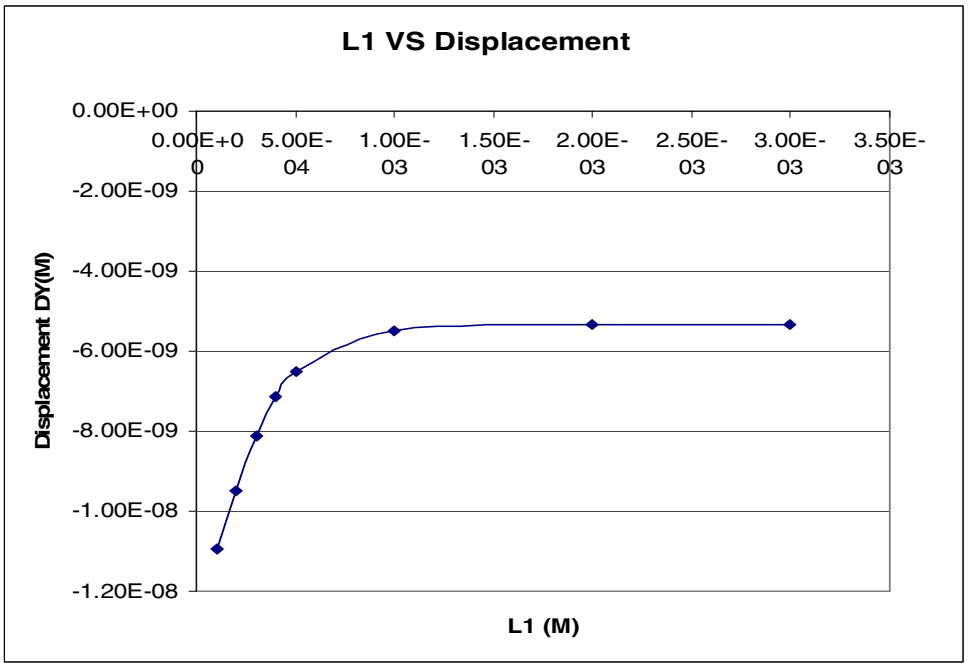

Fig. 50 Displacement sensitivity to thickness in Y-direction

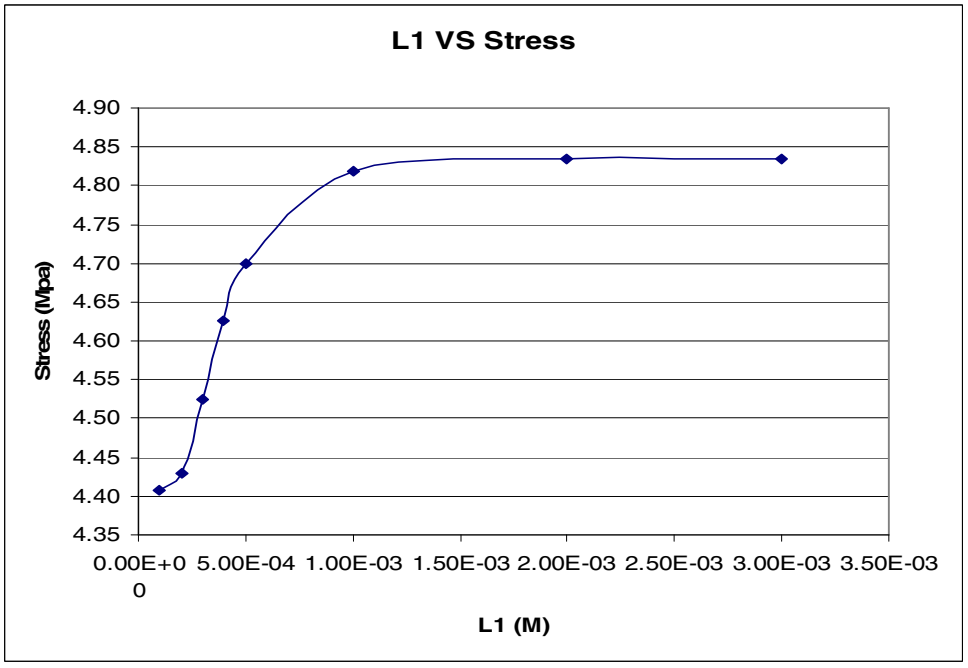

Fig. 51 Stress sensitivity to L1

In Table 16, when comparing shear mode and mono beam by the same model dimensions, the displacement of the shear mode is larger than the displacement of the mono beam by approximately 70 times. The results indicate that the shear mode beam still has better amplifying ability.

Table 16 Comparison between Shear Mode and Normal Mode

TYPE	DX(M)	DY(M)	DZ(M)	Stress (MPa)
Shear mode (Fig. 44)	2.09E-07	-8.75E-09	-2.64E-17	4.47
mono Beam (Fig. 10)	2.97E-09	-8.19E-08	1.64E-09	0.84

3.4 Combination Mode

To increase the tip displacement, a combination mode offers a better way than the mono beam. It is proposed that the displacement could increase if a combination mode of actuation is employed as shown in Fig. 52.

3.4.1 Combination Beam Model 1

The piezoelectric actuator is combined by two parts as Fig. 52 and Fig. 53, with the applied voltages being similar to the shear mode as section 3.3. The sensitivity on the displacement and stress due to changes on T2 are studied.

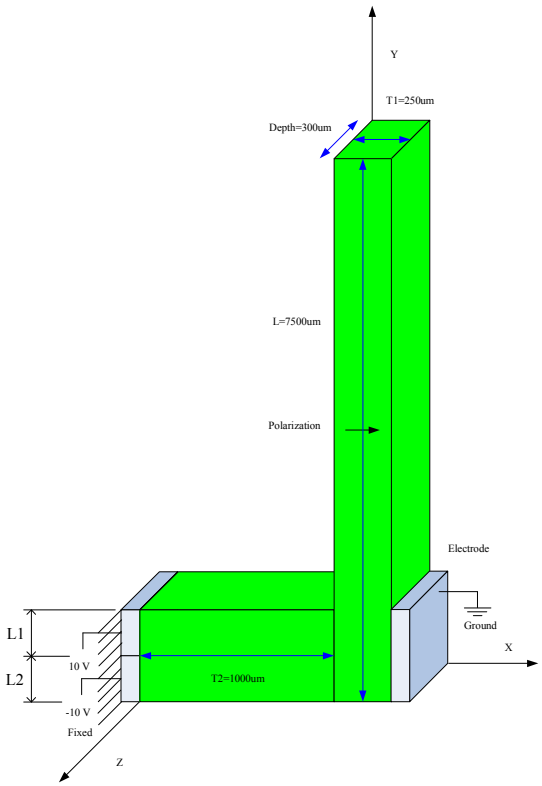

Fig. 52 Geometry, variables and applied voltage for combination model

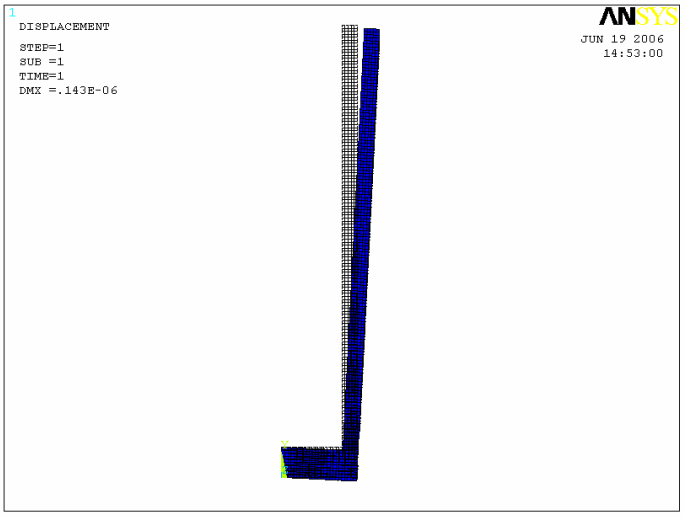

Fig. 53 Combination beam's simulation

In this model, the shear mode concept will be utilized. From Table 17 and Fig. 54-56, when T2 increases over 500 um, the displacement in X-direction and stress reach steady values of 0.141um and 3.21 MPa approximately.

Table 17 Changing T2 of the Actuator

T2(M)	DX(M)	DY(M)	DZ(M)	Stress (MPa)
2.50E-04	1.44E-07	-1.09E-08	3.03E-17	3.21
5.00E-04	1.41E-07	-1.57E-08	1.47E-17	3.21
7.50E-04	1.41E-07	-2.05E-08	1.82E-17	3.21
1.00E-03	1.41E-07	-2.54E-08	1.14E-17	3.21
1.25E-03	1.41E-07	-3.02E-08	2.16E-17	3.21
1.50E-03	1.41E-07	-3.50E-08	2.15E-17	3.21
2.00E-03	1.41E-07	-4.47E-08	4.31E-17	3.21
3.00E-03	1.41E-07	-6.41E-08	-3.32E-17	3.21

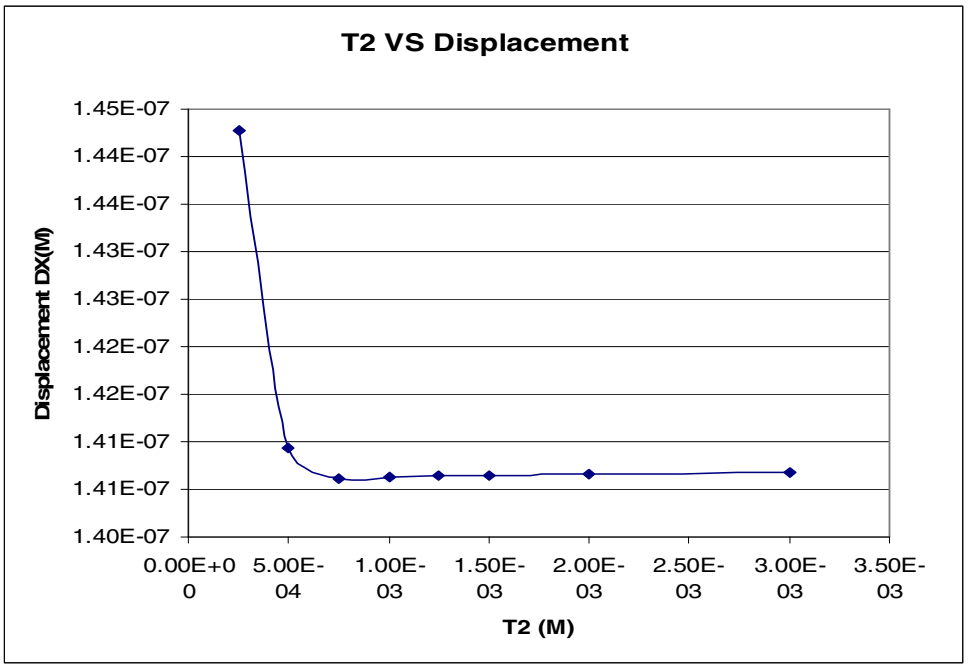

Fig. 54 Displacement sensitivity to T2 in X-direction

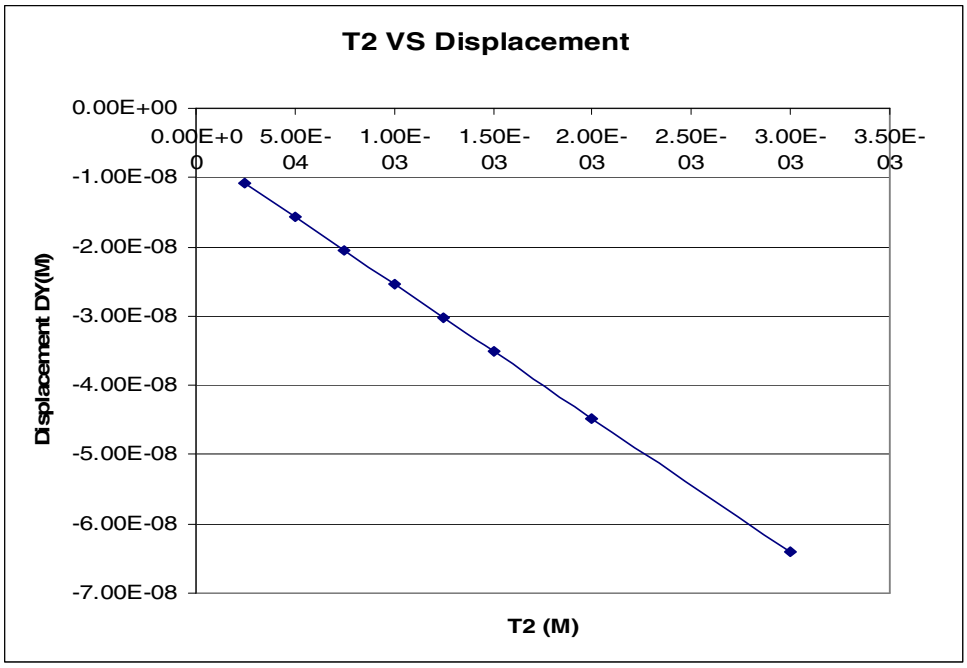

Fig. 55 Displacement sensitivity to T2 in Y-direction

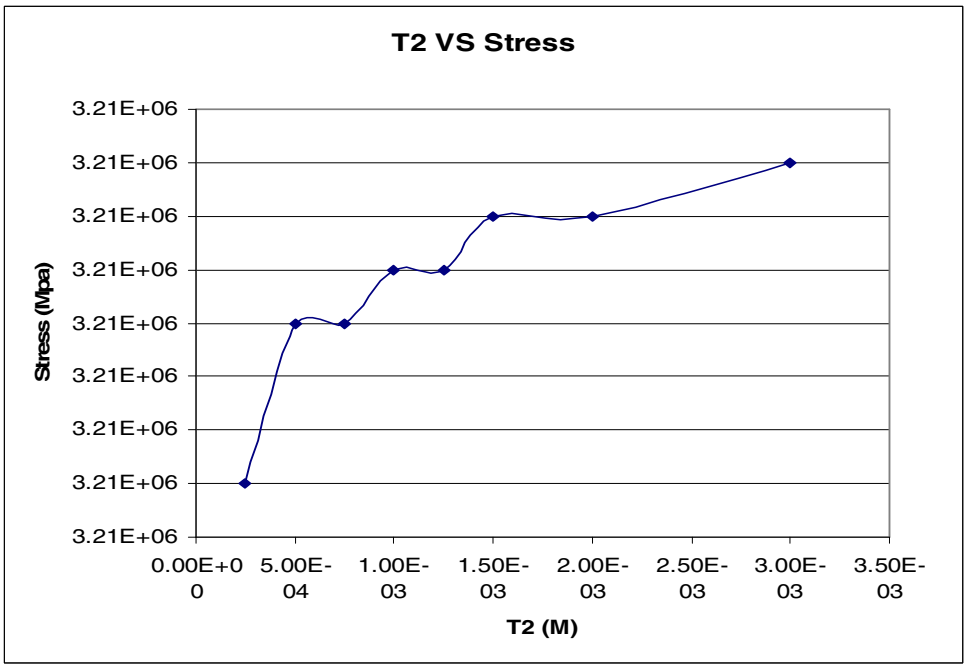

Fig. 56 Stress sensitivity to T2

3.4.2 Combination Beam Model 2

The objective is to identify and analyze concepts that will increase the displacement through bending action. The bending action could be produced by the polarization effect studied in section 3.1.4 and by the shear mode effect studied in section 3.3. In this section, a new design will be explored where both the polarization and shear effects will be combined. This design has a cut out (flute) at the base to reduce the thickness of the beam. However, even if the applied voltage of the combination beam model 1 (3.4.1) can generate a displacement of about 0.14 um, it would not possibly be easily manufactured using the femtosecond laser micromachining system because L1 and L2 are so close as shown in Fig. 52. In addition, the combined geometry, variables and applied voltage are shown in Fig. 57.

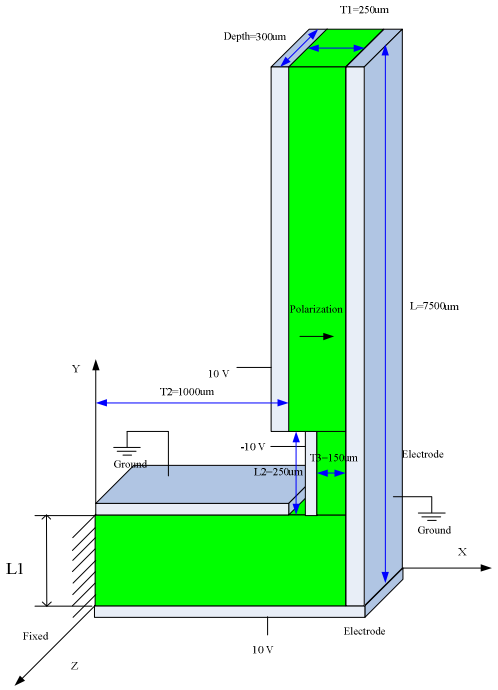

Fig. 57 Geometry, variables and applied voltage

The effects on performance of the five variables, T1 (250 um), T2 (2000 um), T3 (150 um), L1 (250 um), L2 (250 um), will be discussed. By changing the values for one of the variables the displacement sensitivity to that variable is studied.. Subsequently, the parameters with major contribution on the displacement can be easily inferred.

Table 18 Changing T1 of the Actuator

T1(M)	DX(M)	DY(M)	Stress(MPa)
2.00E-04	2.68E-07	5.34E-08	3.90
2.50E-04	2.67E-07	3.23E-08	1.42
3.00E-04	2.66E-07	1.79E-08	1.14
3.50E-04	2.66E-07	7.23E-09	1.13
4.00E-04	2.64E-07	-1.03E-09	1.13
4.50E-04	2.64E-07	-7.71E-09	1.13
5.00E-04	2.63E-07	-1.33E-08	1.13

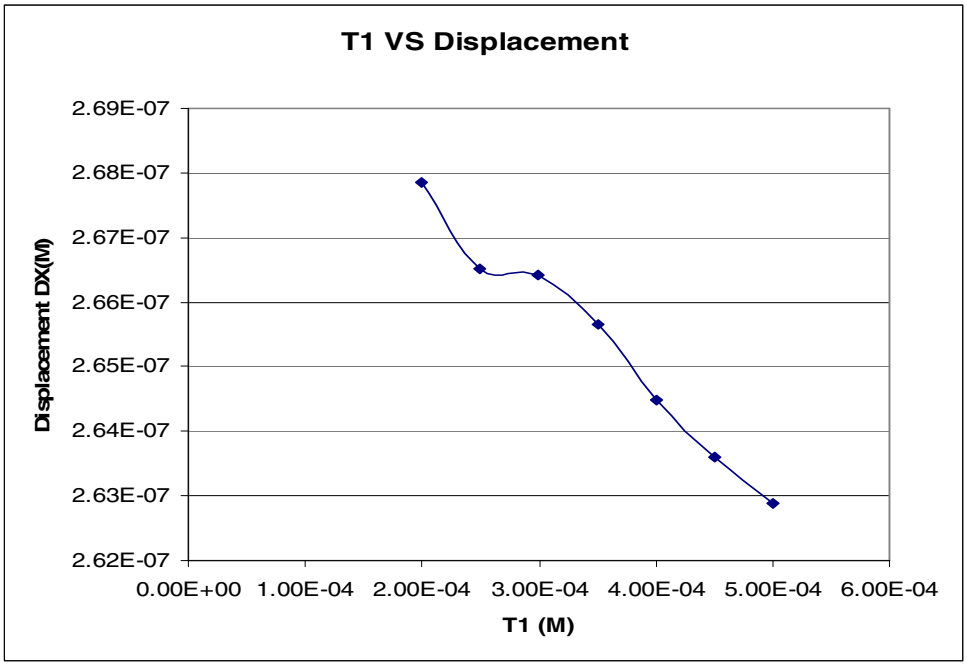

Fig. 58 Displacement sensitivity to T1 in X-direction

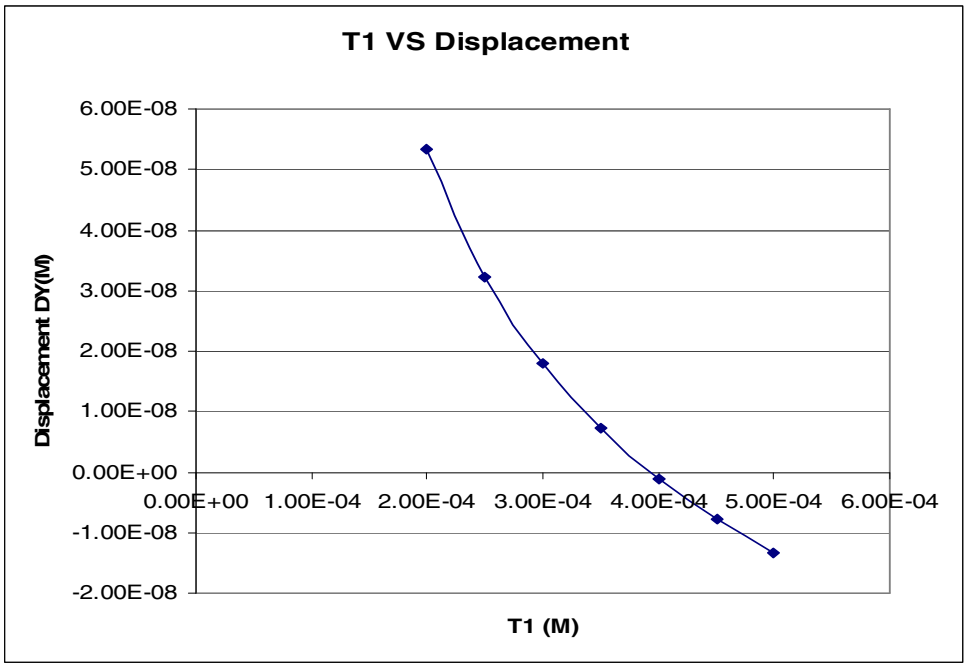

Fig. 59 Displacement sensitivity to T1 in Y-direction

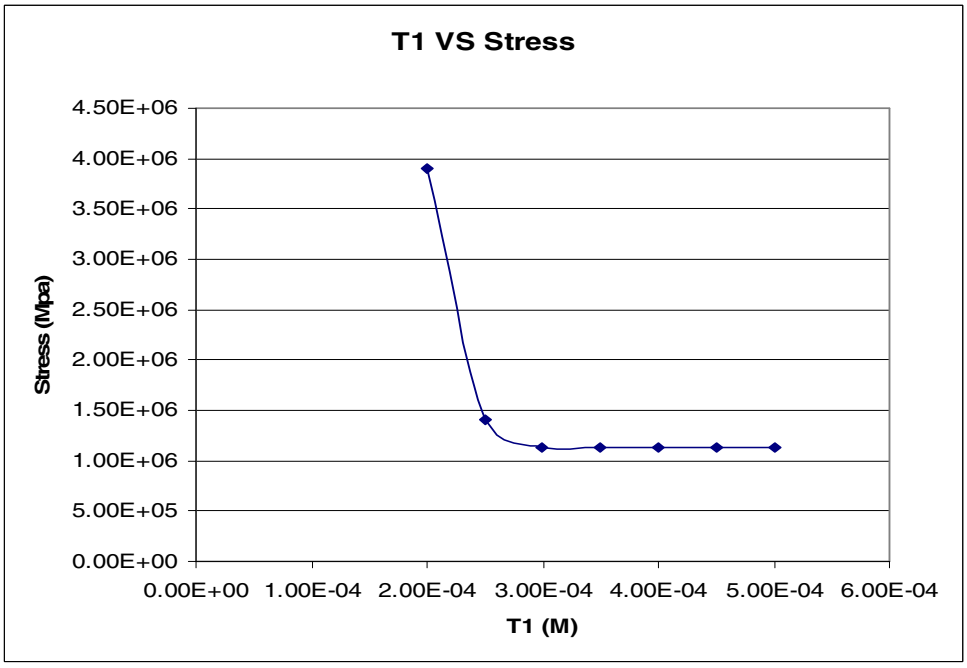

Fig. 60 Stress sensitivity to T2

Table 19 Changing T2 of the Actuator

T2(M)	DX(M)	DY(M)	Stress(MPa)
5.00E-04	2.66E-07	4.71E-08	1.42
1.00E-03	2.66E-07	3.23E-08	1.42
1.50E-03	2.66E-07	1.75E-08	1.42
2.00E-03	2.66E-07	2.68E-09	1.42
2.50E-03	2.66E-07	-1.21E-08	1.42
3.00E-03	2.66E-07	-2.70E-08	1.42

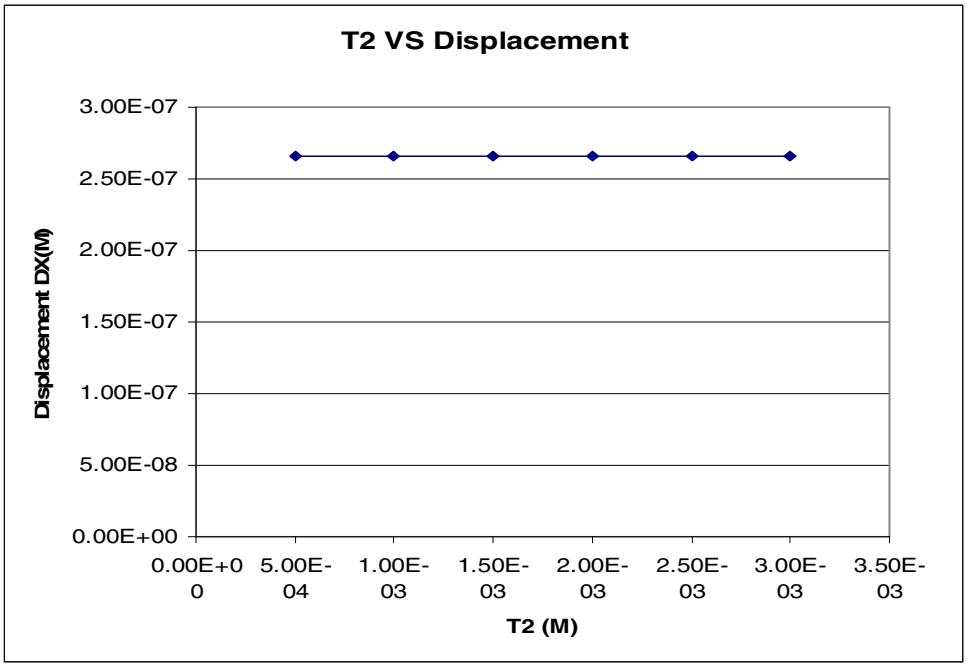

Fig. 61 Relation between T2 and displacement in X-direction

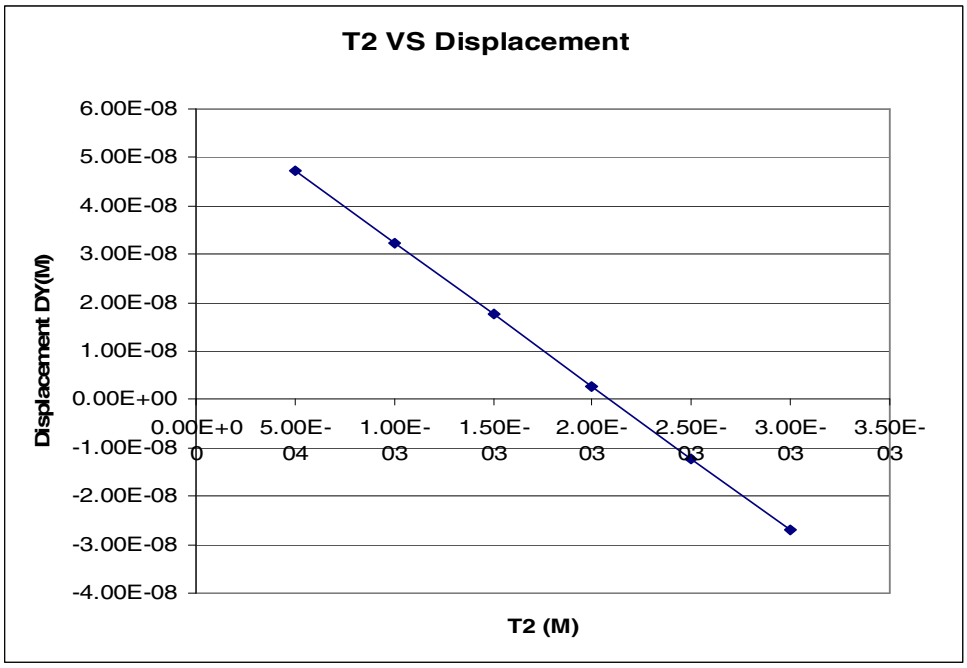

Fig. 62 Relation between T2 and displacement in Y-direction

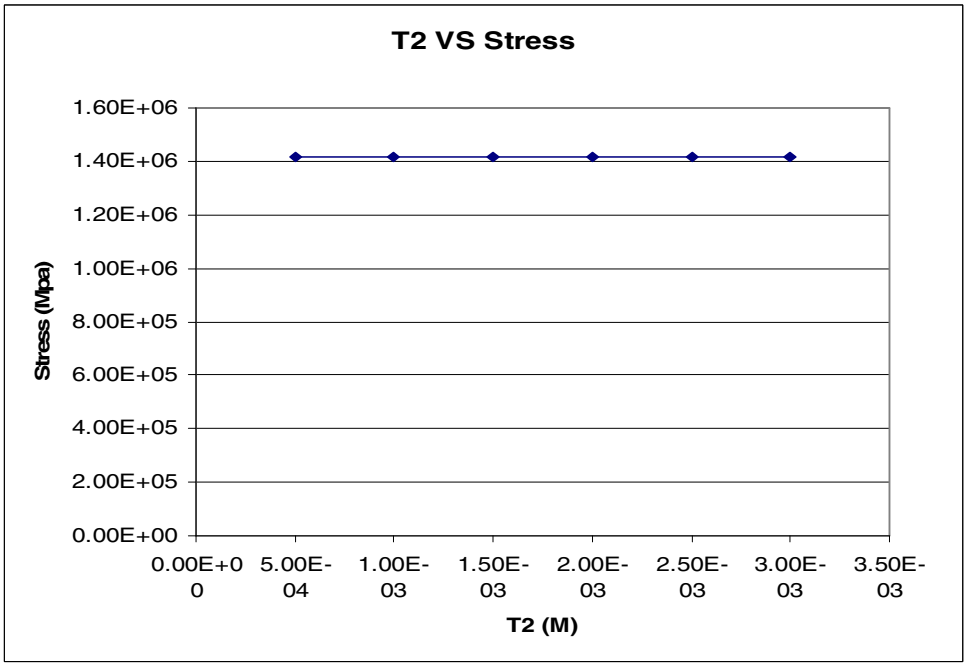

Fig. 63 Relation between T2 and stress

Table 20 Changing T3 of the Actuator

T3(M)	DX(M)	DY(M)	Stress(MPa)
5.00E-05	9.53E-07	-9.96E-09	2.16
1.00E-04	3.70E-07	-6.34E-10	1.19
1.50E-04	2.66E-07	2.68E-09	1.42
2.00E-04	2.31E-07	4.65E-09	3.87
2.50E-04	1.43E-07	3.82E-09	2.01

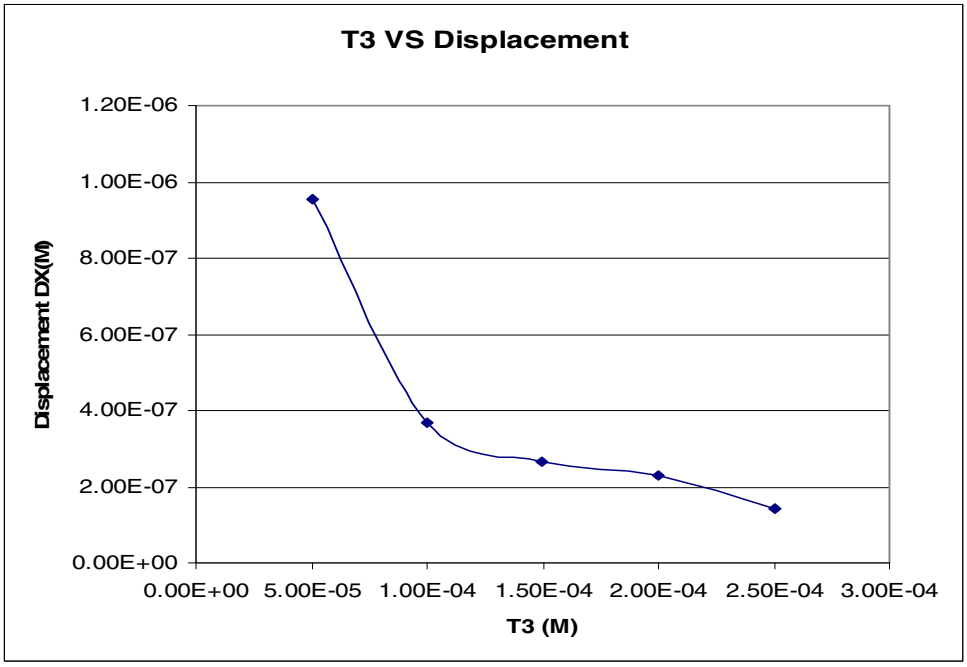

Fig. 64 Relation between T3 and displacement in X-direction

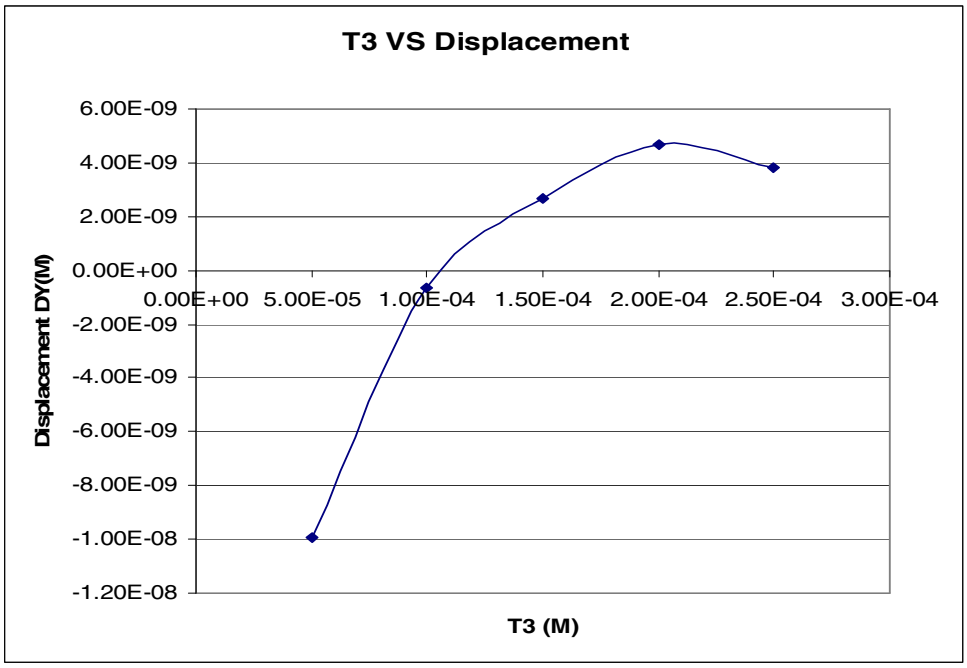

Fig. 65 Relation between T3 and displacement in Y-direction

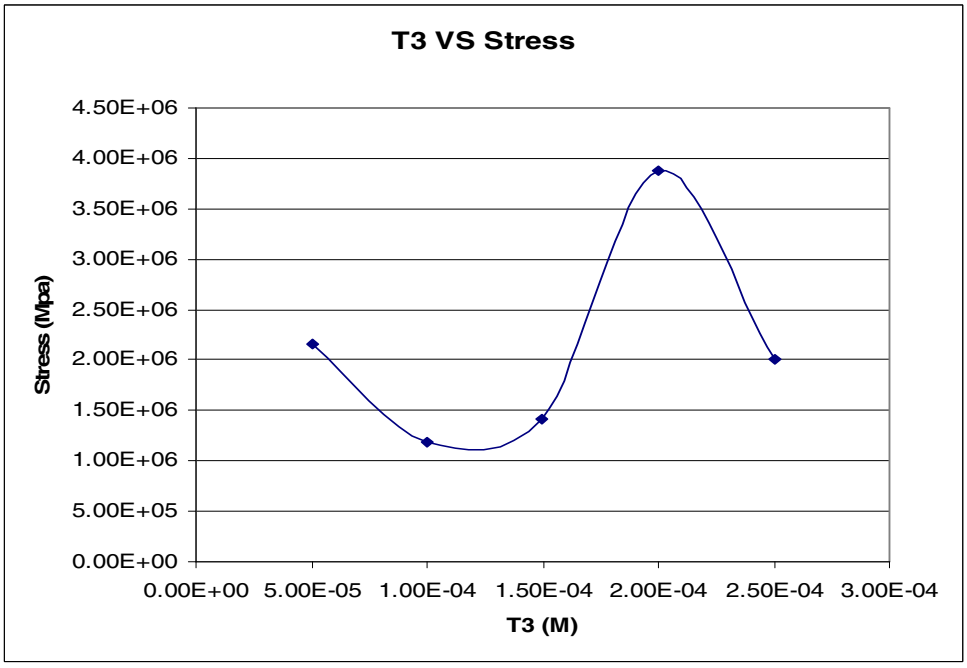

Fig. 66 Relation between T3 and stress

Table 21 Changing L1 of the Actuator

L1 (M)	DX(M)	DY(M)	Stress(MPa)
1.00E-04	6.33E-07	-9.77E-08	1.41
1.50E-04	4.18E-07	-4.14E-08	1.41
2.00E-04	3.21E-07	-1.37E-08	1.42
2.50E-04	2.66E-07	2.68E-09	1.42
3.00E-04	2.32E-07	1.33E-08	1.42
3.50E-04	2.08E-07	2.08E-08	1.42
4.00E-04	1.91E-07	2.62E-08	1.42
4.50E-04	1.77E-07	3.03E-08	1.42
5.00E-04	1.67E-07	3.35E-08	1.42

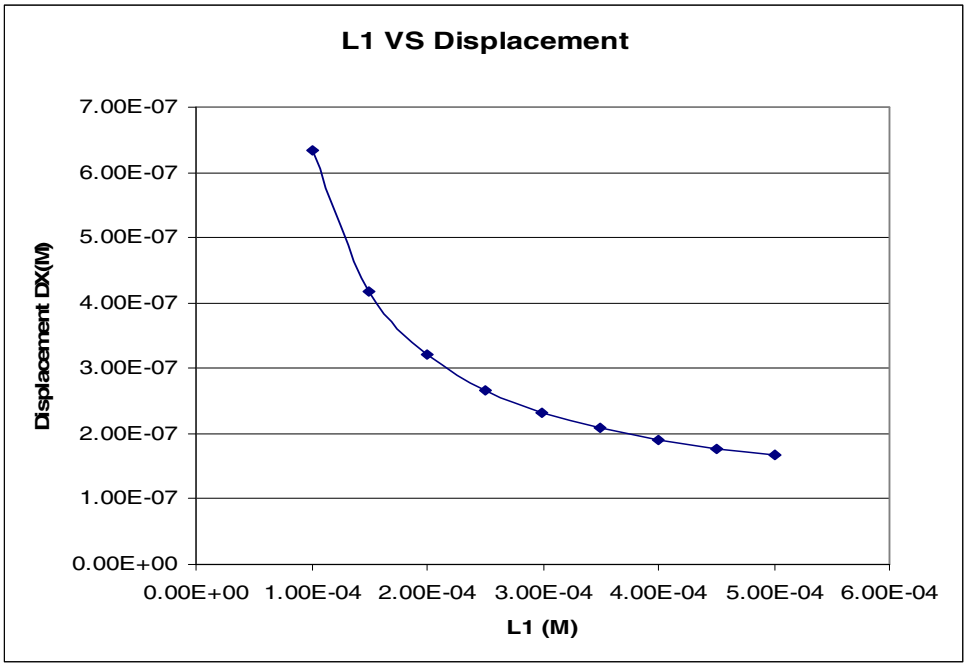

Fig. 67 Relation between L1 and displacement in X-direction

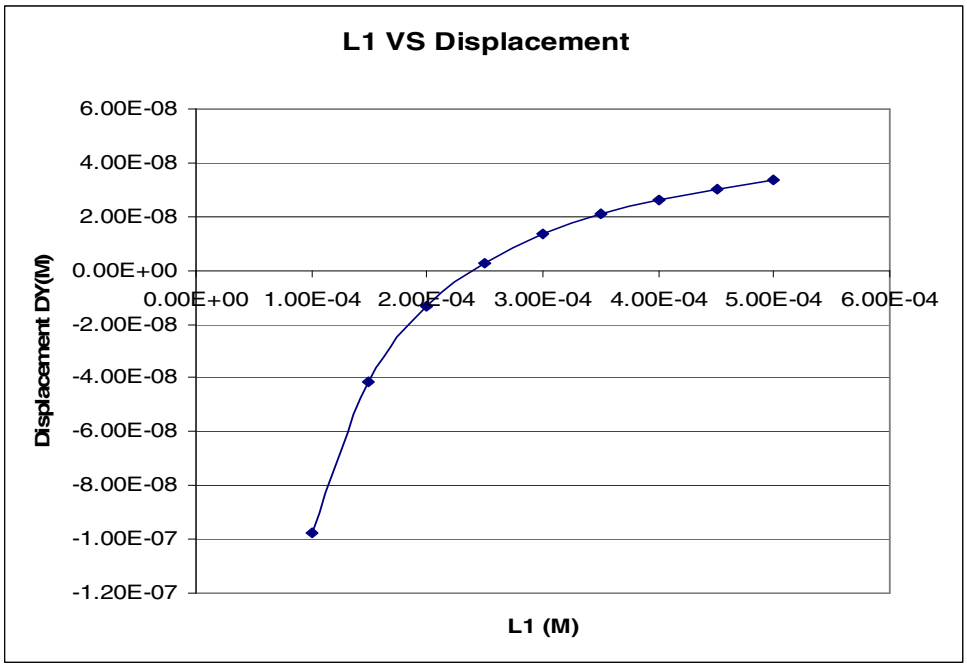

Fig. 68 Relation between L1 and displacement in Y-direction

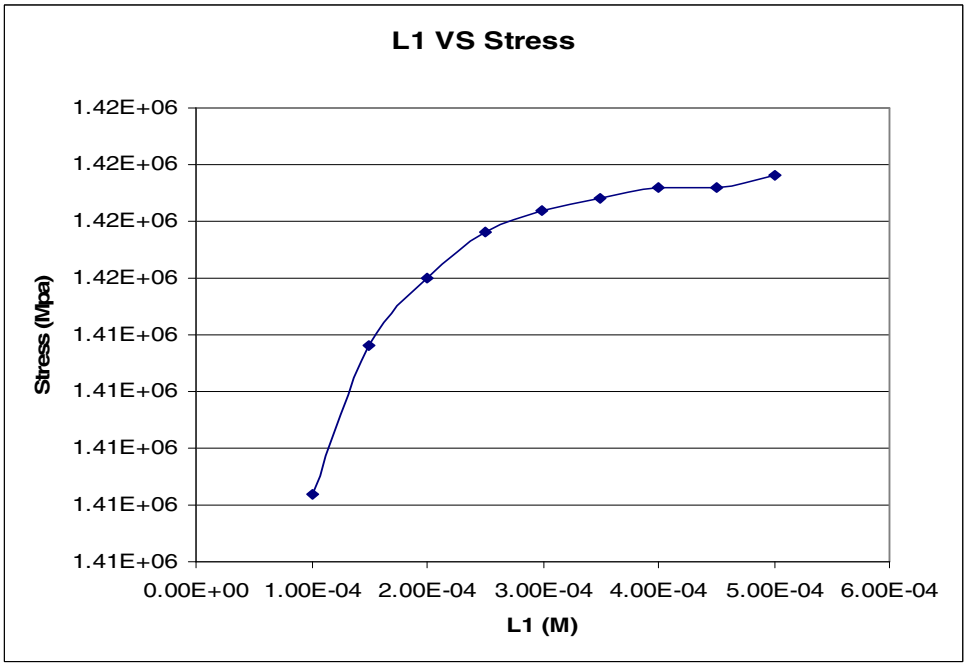

Fig. 69 Relation between L1 and stress

Table 22 Changing L2 of the Actuator

L2 (M)	DX(M)	DY(M)	Stress(MPa)
2.50E-04	2.66E-07	2.68E-09	1.42
5.00E-04	2.64E-07	-4.62E-09	1.42
7.50E-04	2.63E-07	-1.19E-08	1.42
1.00E-03	2.61E-07	-1.92E-08	1.42
1.25E-03	2.59E-07	-2.65E-08	1.42
1.50E-03	2.57E-07	-3.38E-08	1.42
1.75E-03	2.55E-07	-4.12E-08	1.42
2.00E-03	2.53E-07	-4.85E-08	1.42

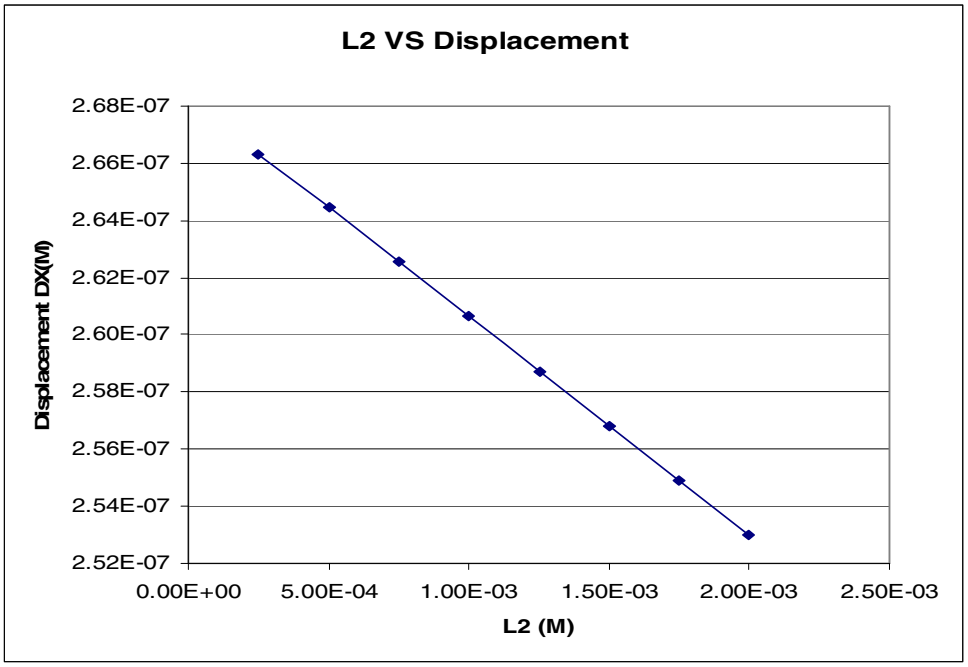

Fig. 70 Relation between L2 and displacement in X-direction

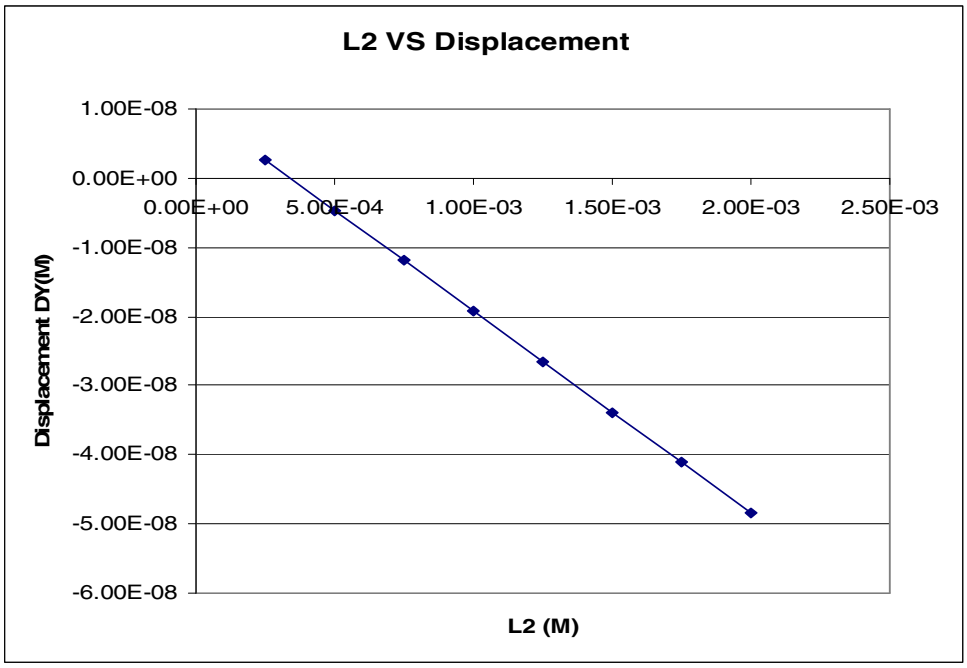

Fig. 71 Relation between L2 and displacement in Y-direction

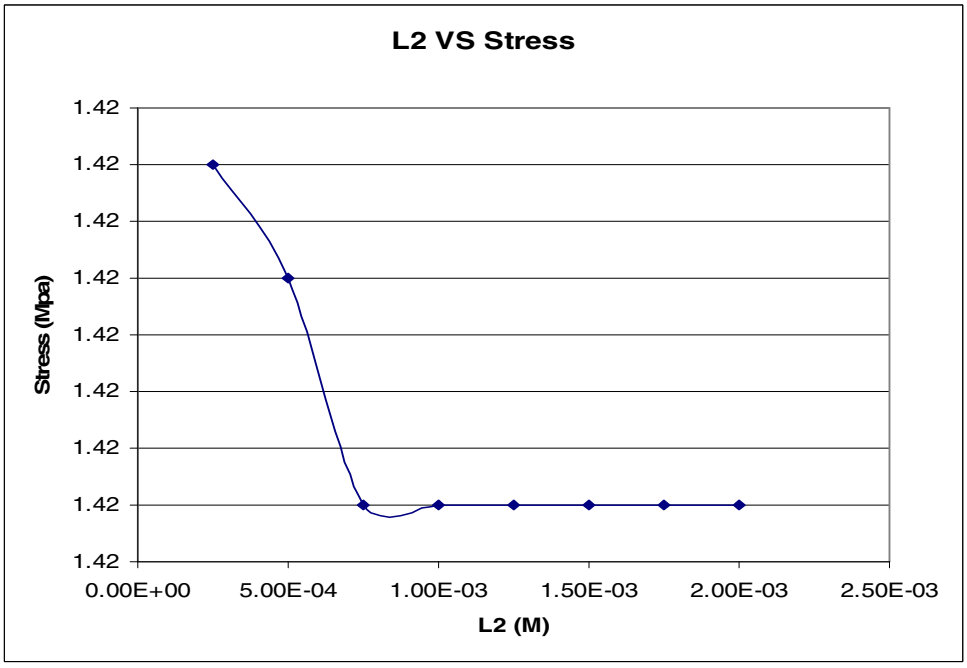

Fig. 72 Relation between L2 and stress

From section 3.4.2 (Table 18 – 22), the qualitative relationships among T1, T2, T3, L1, L2 and the displacement in X-direction can be inferred and shown in Table 23. Regardless of the stress conditions, when T1, T3, L1, L2 are smallest, the displacement will be largest. However, changes on T2 do not have any effect on the displacement.

Table 23 Qualitative Relationship among T1, T2, T3, L1, L2, and Displacement

Variables	Value	Effect to the Deformation	Value	Effect to the Deformation
T1	↑	↓	↓	↑
T2	↑	No Effect	↓	No Effect
T3	↑	↓	↓	↑
L1	↑	↓	↓	↑
L2	↑	↓	↓	↑

It is already discussed that the shear force mode can increase the displacement in X-direction, and the effect of adding the flutes will be discussed in this section. Now, L (7500 um), T1 (250 um), T2 (2000 um), T3 (150 um) Depth (300 um), L1 (250 um), and L2 (250 um) will be fixed, but the number of flutes will changed from 1 to 10. The results are shown in Table 24 indicating a substantial increase in the displacement both in X- and Y-direction.

Table 24 Effect of Number of Flutes on the Actuator Displacement

NUMBER	DX(M)	DY(M)	Stress(MPa)
0	1.43E-07	3.82E-09	2.01
1	2.66E-07	2.68E-09	1.42
2	3.59E-07	-8.42E-09	1.42
3	4.44E-07	-1.95E-08	1.42
4	5.22E-07	-3.06E-08	1.42
5	5.94E-07	-4.17E-08	1.42
10	8.46E-07	-9.73E-08	1.42

3.5 Optimization

In this section, the objective is to use the design optimization procedure in ANSYS to modify the dimensions of the piezoelectric actuator in order to minimize the 1st principal stress and maximize the displacement. The step-by-step procedure is presented in Appendix C and uses the ANSYS GUI (Graphic User Interface) environment. [16] There are several parameters that must be defined.

Design Variables:

250 um $\leq$ L2 $\leq$ 500 um

150 um $\leq$ T3 $\leq$ 250um

State Variable:

The maximum of 1st principal stress (ST) is 60 MPa

Design Objective:

Displacement (DX)

The results indicate that when T3 and L2 are the smallest, the displacement is the largest. The results predicted in Table 23 is the same as the result by optimization results (Table 25)

Table 25 Optimization Results in ANSYS

	SET 1	SET 2	SET 3	SET 4	SET 5
	FEASIBLE	FEASIBLE	FEASIBLE	FEASIBLE	FEASIBLE
ST (SV)	1.4480E+08	3.5557E+08	5.8249E+08	4.3159E+08	1.7789E+08
L2 (DV)	2.5000E-04	4.6179E-04	3.4700E-04	3.8439E-04	2.5036E-04
T3 (DV)	1.5000E-04	1.9115E-04	2.1231E-04	2.0561E-04	1.5014E-04
DX (OBJ)	-2.7224E-07	-2.2621E-07	-2.2573E-07	-2.2597E-07	-2.5349E-07

CHAPTER 4

CONCLUSION AND FUTURE WORK

In this research work, the behavior of piezoelectric actuator under various actuation modes is studied by modeling the behavior in ANSYS. The effect on the performance of the piezo actuator to changes on the dimensions and polarization direction were studied. It was found that a combination mode would substantially increase the tip displacement. In addition, the optimization capabilities in ASNYS were employed in order to simplify the design procedure.

It is recommended that the designed micro actuator be fabricated and characterized and its performance evaluated in order to validate the theoretical analysis and also modify the geometry parameters. The theoretical analysis because the result is related with the applied voltage linearly in ANSYS, an open loop controller should suffice for motion control. However, the bending motion typically achieves nonlinear amplification so a PI controller should be investigated for the open loop controller.

APPENDIX A

A SAMPLE ANSYS CODE AND THE PARAMETERS INITIALIZATION FOR ANSYS

By importing the codes in the text format to substitute the GUI processes in ANSYS, it is easy to change the parameters such as s11, d15, k13 and so on, when changing the piezoelectric materials and parameters. The codes showed below present how to initial the parameters in ANSYS and how to define the parameters.

```
/prep7
/com,
/com,   - compliance coefficients, m2/n
/PZT-5H
antype, static
s11=16.5e-12
s12=-4.78e-12
s13=-8.45e-12
s33=20.7e-12
s44=43.5e-12
s66=2*(s11-s12)
/com,  - piezoelectric strain coefficients, c/n
d15=7.41e-10
d31=-2.74e-10
d33=5.93e-10
/com,  - relative permittivity at constant stress
k11=3130
```

```
k33=3400
/com,  - density, kg/m3
rho=7500
mp,dens,1,rho

/com,  -- material matrices (polar axis along x-axis): ieee input
/com,         x     y   z   xy yz xz              x    y   z
/com,  x   [s33 s13 s13  0  0  0 ]    x     [d31  0    0  ]     [k33  0    0  ]
/com,  y   [s13 s11 s12  0  0  0 ]    y     [d33  0    0  ]     [  0  k33  0  ]
/com,  z   [s13 s12 s11  0  0  0 ]    z     [d31  0    0  ]     [  0   0   k11]
/com,  xy [  0    0    0  s66 0  0 ]    xy    [  0    0    0  ]
/com,  yz [  0    0    0   0 s44 0 ]    yz    [  0    0  d15]
/com,  xz [  0    0    0   0  0 s44]     xz    [  0  d15  0  ]

/com,
/com,  -- material matrices (polar axis along x-axis): ansys input
/com,          x      y   z   xy yz xz              x    y   z
/com,  x   [s33 s13 s13  0  0   0  ]     x   [d33  0   0  ]     [k33  0    0  ]
/com,  y   [s13 s11 s12  0  0   0  ]     y   [d31  0   0  ]     [  0  k11  0  ]
/com,  z   [s13 s12 s11  0  0   0  ]     z   [d31  0   0  ]     [  0   0   k11]
/com,  xy [  0    0    0  s44 0   0  ]     xy [  0  d15 0  ]
/com,  yz [  0    0    0    0 s66 0  ]     yz [  0    0   0  ]
```

/com, xz [0 0 0 0 0 s44] xz [0 0 d15]

tb,anel,1,,,1 ! anisotropic elastic compliance matrix

!0 -- elasticity matrix used as supplied (input in stiffness form).[c]

!1 -- elasticity matrix inverted before use (input in flexibility form).

!this option is not valid for explicit dynamic elements.

tbda,1,s33,s13,s13

tbda,7,s11,s12

tbda,12,s11

tbda,16,s44

tbda,19,s66

tbda,21,s44

tb,piez,1,,,1 !piezoelectric strain matrix

!0 -- piezoelectric stress matrix [e] (used as supplied)

!1 -- piezoelectric strain matrix [d] (converted to [e] form before use)

tbda,1,d33

tbda,4,d31

tbda,7,d31

tbda,11,d15

tbda,18,d15

mp,pery,1,k11

```
mp,perz,1,k11
mp,perx,1,k33              ! Relative permittivity (x direction)
antype,static
et,1,solid5,3               ! 3-d coupled-field solid, piezo option
```

APPENDIX B

A SAMPLE FILE USED IN THE FINITE ELEMENT ANALYSIS SOFTWARE ANSYS

This is a sample file used in Finite Element Analysis software ANSYS. In the front part of the file, it is necessary to initialize the piezoelectric parameters as Appendix B, and after that, the modeling will be designed and created. By importing the file, it is easy to adjust the dimensions and parameters of the models to reduce time.

```
/prep7
/com,
/com,   - compliance coefficients, m2/n
/PZT-5H
antype, static
s11=16.5e-12
s12=-4.78e-12
s13=-8.45e-12
s33=20.7e-12
s44=43.5e-12
s66=2*(s11-s12)
/com,  - piezoelectric strain coefficients, c/n
d15=7.41e-10
d31=-2.74e-10
d33=5.93e-10
/com,  - relative permittivity at constant stress
k11=3130
```

```
k33=3400
/com,  - density, kg/m3
rho=7500
mp,dens,1,rho

/com,  -- material matrices (polar axis along x-axis): ieee input
/com,         x     y   z   xy yz xz              x    y   z
/com,  x   [s33 s13 s13  0  0  0 ]    x     [d31  0    0  ]     [k33  0    0  ]
/com,  y   [s13 s11 s12  0  0  0 ]    y     [d33  0    0  ]     [  0  k33  0  ]
/com,  z   [s13 s12 s11  0  0  0 ]    z     [d31  0    0  ]     [  0   0   k11]
/com,  xy [  0    0    0  s66 0  0 ]    xy    [  0    0    0  ]
/com,  yz [  0    0    0   0 s44 0 ]    yz    [  0    0  d15]
/com,  xz [  0    0    0   0  0 s44]     xz    [  0  d15  0  ]

/com,
/com,  -- material matrices (polar axis along x-axis): ansys input
/com,          x      y   z   xy yz xz              x    y   z
/com,  x   [s33 s13 s13  0  0   0  ]     x   [d33  0   0  ]     [k33  0    0  ]
/com,  y   [s13 s11 s12  0  0   0  ]     y   [d31  0   0  ]     [  0  k11  0  ]
/com,  z   [s13 s12 s11  0  0   0  ]     z   [d31  0   0  ]     [  0   0   k11]
/com,  xy [  0    0    0  s44 0   0  ]     xy [  0  d15 0  ]
/com,  yz [  0    0    0    0 s66 0  ]     yz [  0    0   0  ]
```

/com, xz [0 0 0 0 0 s44] xz [0 0 d15]

tb,anel,1,,,1 ! anisotropic elastic compliance matrix

!0 -- elasticity matrix used as supplied (input in stiffness form).[c]

!1 -- elasticity matrix inverted before use (input in flexibility form).

!this option is not valid for explicit dynamic elements.

tbda,1,s33,s13,s13

tbda,7,s11,s12

tbda,12,s11

tbda,16,s44

tbda,19,s66

tbda,21,s44

tb,piez,1,,,1 !piezoelectric strain matrix

!0 -- piezoelectric stress matrix [e] (used as supplied)

!1 -- piezoelectric strain matrix [d] (converted to [e] form before use)

tbda,1,d33

tbda,4,d31

tbda,7,d31

tbda,11,d15

tbda,18,d15

mp,pery,1,k11

```
mp,perz,1,k11
mp,perx,1,k33              ! Relative permittivity (x direction)
antype,static
et,1,solid5,3              ! 3-d coupled-field solid, piezo option
! modeling design
L1=250E-6
L2=250E-6
L=7500E-6
T1=250E-6
T2=1000E-6
T3=150E-6
WIDTH=300E-6
BLOCK,T2,T2+T1,O,L2,0,WIDTH
BLOCK,T1-T3+T2,T1+T2,L1,L1+L2,0,WIDTH
BLOCK,T2,T1+T2,L1+L2,L,0,WIDTH
BLOCK,0,T2,0,L1,0,WIDTH
VGLUE,ALL
esize,50e-6                !Mesh size
MSHK,1                     ! MAPPED VOLUME MESH
MSHA,0,3D                  ! USING HEX
MAT,1
VSWEEP,All
```

```
DA,23,UX,0              !boundary condition
DA,23,UY,0
DA,23,UZ,0
DA,6,VOLT,0
DA,30,VOLT,0
DA,36,VOLT,0
DA,17,VOLT,-10
DA,11,VOLT,10

DA,28,VOLT,0
DA,27,VOLT,-10
DA,3,VOLT,-10

/SOLU  ! Analyze the modeling
solve
```

APPENDIX C

OPTIMIZATION PORCESSES IN ANSYS

The following is the step-by-step procedure for the piezoelectric actuator using the ANSYS GUI (Graphic User Interface) environment.

Load the actuator code form file

File

Read Input from file (appendix B)

Review the results for displacement

General Post Proc

Plot Results

Contour Plot

Nodal Solution

DOF Solution & X-Component of displacement & OK

List Results

Sorted Listing

Sort Nodes

Dof solution & Translation UX & OK

Create result tables for displacement

(Go to Utility Menu)

Parameters

Get Scalar Data

Results Data & Other operations & OK

Name of Parameter to be defined: DX

From sort oper'n & Minimum value

OK

Review the results for stress

General Post Proc

Plot Results

Contour Plot

Nodal Solution

Stress & 1st Principal stress & OK

List Results

Sorted Listing

Sort Nodes

KABS Sort on absolute value? Click Yes

Stress & 1st Principal stress & OK

Create result tables for stress

(Go to Utility Menu)Parameters

Get Scalar Data

Results Data & Other operations & OK

Name of Parameter to be defined: ST

From sort oper'n & Maximum value

OK

Write the optimization result in the log file

File

Write DB Log File

Enter “actuator” & OK

Setup the optimization process

(Go to Main Menu)

Design Opt

Analysis File

Create & OK

Assign

Type “actuator” & OK

Design variables, state variables, and objective

Design Variables

Add

Parameter name: T3

MIN = 250 E-6

MAX = 500 E-6 & Apply

Parameter name: L2

MIN = 250 E-6

MAX = 500 E-6 & OK

Close

State Variables

Add

Parameter name: ST

MAX = 60E6 & OK

Close

Objective

Add

Parameter name: DX & OK

Close

Design variables, state variables, and objective

Method/Tool

Select Sub-Problem & OK

Maximum Iterations = 30

Max infeasible sets = 15 & OK

Run optimization process

Run & OK

Results

Design Sets

List & OK

REFERENCES

1. Nitin Uppal (2005), Femtosecond Laser micromachining of engineering materials: process parameters study and microrapid prototyping, The University of Texas at Arlington, ,Texas, USA,
2. Roger G. Gilbertson, and John D. Busch (1996), A Survey of Micro-Actuator Technologies for Future Spacecraft Missions, The Journal of The British Interplanetary Society, San Rafael, USA, Vol. 49, pp. 129-138.
3. Michael J. Sinclair (2000), "A High Force Low Area MEMS Thermal Actuator", Thermal and Thermomechanical Phenomena in Electronic Systems. ITHERM 2000. The Seventh Intersociety Conference on Thermal Phenomena., WA, USA Vol. 1, pp. 132, 2000
4. Hui Guo, and Haixia Zhang (2004), "A Novel Electro-Thermal Actuated Micro Position Lock", Solid-State and Integrated Circuits Technology, 2004. Proceedings. 7th International Conference on Solid State and Integrated Circuit Technology (ICSICT 2004), Vol. 3, pp. 1915-1918.
5. Koji Ikuta, Hiroyuki Fujita, Suguru Arimoto, Michiaki Ikeda, and Shinji Yamashita (1990), "Development of Micro Actuator Using Shape Memory Alloy Thin Film", Proceedings of the IEEE International Workshop on Intelligent Robots and Systems (IROS '90), Ibaraki, Japan, pp. 16-19.

6. William C. Tang, Martin G. Lim,* and Roger T. Howe (1990), ”Electrostatically Balanced Comb Drive for Controlled Levitation”, Solid-State Sensor and Actuator Workshop, 1990. 4th Technical Digest., IEEE, SC, USA, pp. 23-27.
7. Ph. Robert (2004), “MEMS Actuation: A Range of Principles and Technologies”, http://www-leti.cea.fr/commun/AR-2004/T3/T3-4.pdf
8. M. C. Wu, “Piezoelectric Transducers”, http://www.ee.ucla.edu/~wu/ee250b/Microsoft%20PowerPoint%20-%20Piezoelectric%20transducers.pdf
9. Christopher Niezrecki, Diann Brei, Sivakumar Balakrishnan, and Andrew Moskalik (2001), “Piezoelectric Actuation: State of The Art”, The Shock and Vibration Digest, Vol. 33, pp. 269-280.
10. James D. Ervin, and Diann Brei (1998), “Recurve Piezoelectric-Strain-Amplifying Actuator Architecture”, IEEE/ASME Transactions on Mechatronics, Vol. 3, No. 4, pp. 293-301
11. Bernard Jaffe, William R. Cook, Jr and Hans Jaffe (1971),“Piezoelectric ceramics”, Bedford, Ohio, USA, 44146 and Cleveland, Ohio, USA, 44108
12. “Piezoelectricity: Overview”, Engineering Fundamentals, http://www.efunda.com/materials/piezo/general_info/gen_info_index.cfm
13. K. K. Tan, and A. S. Putra (2005), ”Partial-rotating piezoelectric actuators for intracytoplasmic sperm injection”, Proceedings of SPIE- the International Society for Optical Engineering, Vol. 6048, pp. 186-194

14. T.L. Jordan, and Z. Ounaies (2001), “Piezoelectric Ceramics Characterization”, ICASE Report No. 2001-28, Virginia, USA
15. ANSYS 9.0 Documentation
16. www.four-h.purdue.edu/ABE450/Extra%20Credit/design_optimization_tutorial_2005.doc

BIOGRAPHICAL INFORMATION

Po-Shiun Chen graduated from National Cheng Kung University whose department of mechanical engineering has the high reputation in Taiwan in 1998. After the B.S education, he serviced in Republic of China Army from 1998 to 2000. In this period of 2001-2003, he proceeded to work in the company, Sunmax Technology Co. Ltd, which is a touch-panel equipment company that focuses on automatic machines and measuring systems, and being an engineer, he learned numerous skills about hardware, software, mechanical design and structure needed to meet production deadlines. He continued his education in University of Texas at Arlington for Masters of Science program in Mechanical Engineering in fall of 2004. He worked in the BioMEMS lab under the supervision of Dr. P.S. Shiakolas in the area about analysis and design of piezoelectric micro-actuator. He received his Master degree in August 2006 and focuses on the researches about design and analysis in MEMS devices.